

# The Maximum Intensity of Tropical Cyclones in Axisymmetric Numerical Model Simulations

GEORGE H. BRYAN AND RICHARD ROTUNNO

*National Center for Atmospheric Research,\* Boulder, Colorado*

(Manuscript received 1 July 2008, in final form 26 November 2008)

## ABSTRACT

An axisymmetric numerical model is used to evaluate the maximum possible intensity of tropical cyclones. As compared with traditionally formulated nonhydrostatic models, this new model has improved mass and energy conservation in saturated conditions. In comparison with the axisymmetric model developed by Rotunno and Emanuel, the new model produces weaker cyclones (by  $\sim 10\%$ , in terms of maximum azimuthal velocity); the difference is attributable to several approximations in the Rotunno–Emanuel model. Then, using a single specification for initial conditions (with a sea surface temperature of  $26^\circ\text{C}$ ), the authors conduct model sensitivity tests to determine the sensitivity of maximum azimuthal velocity ( $v_{\text{max}}$ ) to uncertain aspects of the modeling system. For fixed mixing lengths in the turbulence parameterization, a converged value of  $v_{\text{max}}$  is achieved for radial grid spacing of order 1 km and vertical grid spacing of order 250 m. The fall velocity of condensate ( $V_f$ ) changes  $v_{\text{max}}$  by up to 60%, and the largest  $v_{\text{max}}$  occurs for pseudoadiabatic thermodynamics (i.e., for  $V_f > 10 \text{ m s}^{-1}$ ). The sensitivity of  $v_{\text{max}}$  to the ratio of surface exchange coefficients for entropy and momentum ( $C_E/C_D$ ) matches the theoretical result,  $v_{\text{max}} \sim (C_E/C_D)^{1/2}$ , for nearly inviscid flow, but simulations with increasing turbulence intensity show less dependence on  $C_E/C_D$ ; this result suggests that the effect of  $C_E/C_D$  is less important than has been argued previously. The authors find that  $v_{\text{max}}$  is most sensitive to the intensity of turbulence in the radial direction. However, some settings, such as inviscid flow, yield clearly unnatural structures; for example,  $v_{\text{max}}$  exceeds  $110 \text{ m s}^{-1}$ , despite a maximum observed intensity of  $\sim 70 \text{ m s}^{-1}$  for this environment. The authors show that turbulence in the radial direction limits maximum axisymmetric intensity by weakening the radial gradients of angular momentum (which prevents environmental air from being drawn to small radius) and of entropy (which is consistent with weaker intensity by consideration of thermal wind balance). It is also argued that future studies should consider parameterized turbulence as an important factor in simulated tropical cyclone intensity.

## 1. Introduction

The theoretical maximum intensity of tropical cyclones has been a subject of much study recently. There are several possible applications for this subject, such as for real-time forecasting, for hazard planning and management, and for studying the consequences of climate change. Hence, a reasonable estimate for maximum intensity has clear value.

Several different strategies are used to explore this topic. We classify these approaches into three general

categories. One is the analytic approach, which relies primarily upon the governing equations for the atmosphere and several assumptions about the processes that occur in tropical cyclones. This method has probably received the greatest attention, at least in the published literature. Notable techniques have been put forth recently by Emanuel (1986, 1988, 1995) and Holland (1997). These techniques are commonly referred to as potential intensity (PI) theories.

A second method is to use an entirely observational dataset. In this approach, statistical analysis is used to determine the maximum intensity as a function of observed environmental conditions (e.g., sea surface temperature). This approach was undertaken, for example, by DeMaria and Kaplan (1994), Whitney and Hobgood (1997), and Zeng et al. (2007).

A third method is to use a time-dependent numerical model. In this approach, a weak tropical cyclone is placed

---

\* The National Center for Atmospheric Research is sponsored by the National Science Foundation.

---

Corresponding author address: George H. Bryan, National Center for Atmospheric Research, 3450 Mitchell Lane, Boulder, CO 80301.  
E-mail: gbryan@ucar.edu

into a specified environment; the model is then integrated forward in time, the tropical cyclone intensifies, and ultimately a maximum intensity is achieved. This approach was undertaken, for example, using an axisymmetric numerical model by Rotunno and Emanuel (1987) and Persing and Montgomery (2005).

Of these three approaches, numerical modeling is probably the easiest to undertake, in the sense that little input is required of the model user. For example, as opposed to the analytic approach, numerical modeling does not require a great deal of knowledge about the flow to be studied; rather, given suitable initial and boundary conditions, then the numerical model will generate the flow of interest. Furthermore, as opposed to the observational approach, numerical modeling does not require a large dataset of observations; rather, the maximum intensity can be studied in idealized environments, where only an environmental sounding, a sea surface temperature, and a weak initial vortex need to be specified.

On the other hand, numerical modeling has several potential drawbacks. The governing equations and parameterizations need to accurately describe all important processes that occur in tropical cyclones. The grid spacing must be sufficiently small to resolve the important features of a tropical cyclone, and the effects of unresolved turbulent motions must be included accurately. Additionally, the model's numerical techniques must be sufficiently accurate so they do not affect the solution.

In this article, the maximum intensity of tropical cyclones is investigated using a time-dependent, axisymmetric, nonhydrostatic numerical model. The primary goal is to determine the maximum possible intensity of a tropical cyclone in the numerical model given a single specified set of initial conditions. Additionally, the sensitivity of model-produced maximum intensity is investigated by making changes to components of the model that have uncertain settings: examples include the grid spacing, the turbulence parameterization, the air-sea exchange coefficients, settings in the microphysics parameterization, and the governing equations of the model. The model-produced intensity is compared to the maximum value that has been observed for this environment, which helps identify processes that might be important for determining the maximum intensity of natural tropical cyclones. These results should be useful to numerical model developers, and they can also help guide the development of analytic PI theories.

An axisymmetric model is used herein because its small computational overhead allows us to investigate a large number of modeling components systematically. The primary drawback to axisymmetric models, of course, is the lack of three-dimensional features such as mesovortices in the eye/eyewall, boundary layer roll

vortices, upper-level asymmetric outflow jets, vortex Rossby waves, etc., which must be viewed as turbulence and accounted for by a parameterization. Hence, some results reported herein might be specific to axisymmetric models, and should someday be reevaluated using three-dimensional numerical simulations.

## 2. Description of the numerical model

A new axisymmetric numerical model was developed for this study to take advantage of recent advances in numerical model design. The model is based on the compressible nonhydrostatic cloud model of Bryan and Fritsch (2002). It is configured for axisymmetric simulations of tropical cyclones following the study by Rotunno and Emanuel (1987, hereafter RE87). Compared to the RE87 model, there are several notable improvements in the new model, including an equation set that mathematically conserves total mass and energy in reversible saturated conditions; the ability to include dissipative heating, which has been shown to increase hurricane intensity by as much as 20% (e.g., Bister and Emanuel 1998); and more accurate numerical techniques for split-explicit compressible models (e.g., Wicker and Skamarock 2002). There are, however, several similarities between these two models, including both are compressible nonhydrostatic models; both use the same grid staggering; both use the same general approach for parameterization of turbulence; and, for all simulations in this article, both use the same simple methods to specify radiative and microphysical processes. Further details of the differences are provided below. Readers that are not interested in model details can skip ahead to section 3, which presents the primary results of this study.

### a. Governing equations

The model equations are written in cylindrical coordinates  $(r, \phi, z)$ , although, by assumption, no variation in  $\phi$  is permitted herein. There are seven time-dependent variables: velocities in the radial, azimuthal, and vertical directions  $(u, v, w)$ ; perturbation nondimensional pressure  $\pi'$ ; potential temperature  $\theta$ ; mixing ratio of water vapor  $q_w$ ; and mixing ratio of liquid water  $q_l$ . The governing equations for these variables are as follows:

$$\frac{\partial u}{\partial t} = -u \frac{\partial u}{\partial r} - w \frac{\partial u}{\partial z} + \left(f + \frac{v}{r}\right)v - c_p \theta_v \frac{\partial \pi'}{\partial r} + D_u + N_u, \quad (1)$$

$$\frac{\partial v}{\partial t} = -u \frac{\partial v}{\partial r} - w \frac{\partial v}{\partial z} - \left(f + \frac{v}{r}\right)u + D_v + N_v, \quad (2)$$

$$\frac{\partial w}{\partial t} = -u \frac{\partial w}{\partial r} - w \frac{\partial w}{\partial z} - c_p \theta_v \frac{\partial \pi'}{\partial z} + g \left( \frac{\theta'_v}{\theta_v} \right) + D_w + N_w, \quad \Theta_1 = 0, \text{ and } \Theta_2 = \frac{L_v}{c_p \pi}, \quad (9)$$

$$\frac{\partial \pi'}{\partial t} = -u \frac{\partial \pi}{\partial r} - w \frac{\partial \pi}{\partial z} - \Pi_1 \pi \left( \frac{1}{r} \frac{\partial r u}{\partial r} + \frac{\partial w}{\partial z} \right) + \Pi_2 \dot{q}_{\text{cond}} + \Pi_3 (\epsilon + D_\theta + N_\theta + R), \quad (4)$$

$$\frac{\partial \theta}{\partial t} = -u \frac{\partial \theta}{\partial r} - w \frac{\partial \theta}{\partial z} - \Theta_1 \theta \left( \frac{1}{r} \frac{\partial r u}{\partial r} + \frac{\partial w}{\partial z} \right) + \Theta_2 \dot{q}_{\text{cond}} + \Theta_3 \epsilon + D_\theta + N_\theta + R, \quad (5)$$

$$\frac{\partial q_v}{\partial t} = -u \frac{\partial q_v}{\partial r} - w \frac{\partial q_v}{\partial z} + D_{q_v} - \dot{q}_{\text{cond}}, \quad \text{and} \quad (6)$$

$$\frac{\partial q_l}{\partial t} = -u \frac{\partial q_l}{\partial r} - w \frac{\partial q_l}{\partial z} + D_{q_l} + \dot{q}_{\text{cond}} + \frac{1}{\rho_d} \frac{\partial (\rho_d q_l V_t)}{\partial z}. \quad (7)$$

Overbars refer to a one-dimensional (vertical) reference profile that is in hydrostatic balance [ $d\bar{\pi}/dz = -g/(c_p \bar{\theta}_v)$ ], and primes refer to perturbations from this reference state. The definitions for  $\pi$  and  $\theta$  are customary:  $\pi \equiv (p/p_0)^{R_d/c_p}$  and  $\theta \equiv T/\pi$ , where  $p_0$  is a reference pressure,  $c_p$  is the specific heat of dry air at constant pressure,  $R_d$  is the gas constant for dry air, and  $T$  is absolute temperature. Virtual potential temperature includes the effects of liquid water:  $\theta_v \equiv \theta(1 + q_v R_v/R_d)/(1 + q_v + q_l)$ , where  $R_v$  is the gas constant for water vapor. Other symbols are defined as follows:  $f$  is the Coriolis parameter;  $g$  is gravitational acceleration; the  $D$  symbols represent tendencies from turbulent motions (described below);  $N$  represents upper-level Newtonian damping used to eliminate vertically propagating gravity waves, following RE87 (p. 546);  $R$  is the term from RE87 (p. 546) that mimics radiative cooling throughout the domain;  $\dot{q}_{\text{cond}}$  is the rate of condensation/evaporation between vapor and liquid;  $\rho_d$  is density of dry air, determined using the ideal gas law,  $\rho_d = p_0 \pi^{c_v/R_d} [R_d \theta (1 + q_v R_v/R_d)]^{-1}$ ; and  $V_t$  is the terminal fall velocity of liquid water. The symbols  $\Theta_3$  and  $\epsilon$  are associated with dissipative heating and are explained below.

The remaining undefined symbols— $\Pi_1$ ,  $\Pi_2$ ,  $\Pi_3$ ,  $\Theta_1$ , and  $\Theta_2$ —are associated with the conservation of mass and internal energy in moist flows. These variables can be formulated in two ways. One yields an approximate equation set that is traditionally used for nonhydrostatic cloud models and is very similar to the equations used by RE87:

$$\Pi_1 = \frac{R_d}{c_v}, \quad \Pi_2 = 0, \quad \Pi_3 = 0, \quad (8)$$

where  $L_v$  is the latent heat of vaporization and  $c_v$  is the specific heat of dry air at constant volume. With this formulation, hereafter referred to as the “traditional equation set,” the model cannot conserve mass and internal energy. The second formulation, derived by Bryan and Fritsch (2002) and hereafter referred to as the “conservative equation set,” allows the total mass and internal energy to be conserved in a reversible moist environment, and the appropriate formulations are

$$\Pi_1 = \frac{R_d c_{pm}}{c_p c_{vm}}, \quad \Pi_2 = \frac{R_d}{c_p} \left( \frac{L_v}{c_{vm} \theta} - \pi \frac{R_v c_{pm}}{R_m c_{vm}} \right), \quad \Pi_3 = \frac{R \pi}{c_v \theta}, \quad (10)$$

$$\Theta_1 = \left( \frac{R_m}{c_{vm}} - \frac{R_d c_{pm}}{c_p c_{vm}} \right), \quad \text{and} \quad \Theta_2 = \frac{c_v L_v}{c_{vm} c_p \pi} - \theta \frac{R_v}{c_{vm}} \left( 1 - \frac{R_d c_{pm}}{c_p R_m} \right), \quad (11)$$

where variables for the mixture of moist, saturated air are defined as follows:

$$c_{pm} \equiv c_p + c_{pv} q_v + c_l q_l, \quad c_{vm} \equiv c_v + c_{vv} q_v + c_l q_l, \quad \text{and} \quad R_m \equiv R_d + R_v q_v, \quad (12)$$

and where  $c_{pv}$  and  $c_{vv}$  are the specific heats of water vapor at constant pressure and volume, respectively, and  $c_l$  is the specific heat of liquid water. Using these variables, a governing equation for total mass can be derived by using the ideal gas law, the definitions of mixing ratios, and using (4)–(7); for the conservative equation set, this yields

$$\frac{\partial \rho_t}{\partial t} + \frac{1}{r} \frac{\partial (r \rho_t u)}{\partial r} + \frac{\partial (\rho_t w)}{\partial z} = \frac{\partial (\rho_l V_t)}{\partial z} + D_{q_t}, \quad (13)$$

where  $\rho_t \equiv \rho_d + \rho_v + \rho_l$  is total density [the sum of the densities of dry air ( $\rho_d$ ), water vapor ( $\rho_v$ ), and liquid water ( $\rho_l$ )] and  $D_{q_t}$  represents the tendency from turbulence (which, we note, includes the surface flux of water vapor). It can easily be shown that total mass inside the domain is conserved in the absence of surface precipitation and surface water vapor flux, and that the so-called precipitation mass sink effect [e.g., studied by Qiu et al. (1993) and Lackmann and Yablonsky (2004)] is included in this model when using the conservative equation set. We also note that the conservative equation set reduces to the traditional equation set by setting  $c_{pv} = c_{vv} = c_l = R_v = \Pi_2 = \Pi_3 = 0$ .

The diffusive terms ( $D$ ) in (1)–(7) are tendencies from a parameterization of unrepresented motions (i.e., turbulence). Our formulation is similar to the one used by RE87, although we utilize the deep anelastic equations (instead of the incompressible Boussinesq equations) during our derivation of these terms. These tendencies are formulated as follows:

$$\begin{aligned} D_u &= \frac{1}{r} \frac{\partial r \tau_{rr}}{\partial r} + \frac{1}{\bar{\rho}} \frac{\partial \bar{\rho} \tau_{rz}}{\partial z} - \frac{\tau_{\phi\phi}}{r}, \\ D_v &= \frac{1}{r^2} \frac{\partial r^2 \tau_{r\phi}}{\partial r} + \frac{1}{\bar{\rho}} \frac{\partial \bar{\rho} \tau_{z\phi}}{\partial z}, \\ D_w &= \frac{1}{r} \frac{\partial r \tau_{rz}}{\partial r} + \frac{1}{\bar{\rho}} \frac{\partial \bar{\rho} \tau_{zz}}{\partial z}, \quad \text{and} \\ D_\chi &= -\frac{1}{r} \frac{\partial r F_r^\chi}{\partial r} - \frac{1}{\bar{\rho}} \frac{\partial \bar{\rho} F_z^\chi}{\partial z}, \end{aligned} \quad (14)$$

where  $\chi$  represents one of the model’s scalars ( $\theta$ ,  $q_v$ , or  $q_l$ ). The stresses ( $\tau$ ) and fluxes ( $F$ ) are parameterized as in RE87 (p. 545 for the model’s interior, and p. 547 for the surface). Assuming steady, homogeneous turbulence, we derive a turbulence kinetic energy budget for these equations:

$$\nu_h S_h^2 + \nu_v S_v^2 - \nu_m N_m^2 = \epsilon, \quad (15)$$

where  $\nu$  is an eddy viscosity, subscripts  $h$  and  $v$  refer to effects from unrepresented horizontal and vertical eddy fluxes respectively,  $N_m^2$  is the squared Brunt–Väisälä frequency,  $\epsilon$  is the rate of dissipation of kinetic energy at molecular scales, and  $S^2$  is deformation given by

$$\begin{aligned} S_h^2 &= 2 \left( \frac{\partial u}{\partial r} \right)^2 + 2 \left( \frac{u}{r} \right)^2 + \left( \frac{\partial v}{\partial r} - \frac{v}{r} \right)^2 \quad \text{and} \\ S_v^2 &= 2 \left( \frac{\partial w}{\partial z} \right)^2 + \left( \frac{\partial u}{\partial z} + \frac{\partial w}{\partial r} \right)^2 + \left( \frac{\partial v}{\partial z} \right)^2. \end{aligned} \quad (16)$$

We split the dissipation into two components: one accounting for dissipation of horizontal turbulence motions ( $\epsilon_h$ ), and one accounting for dissipation of vertical turbulence motions ( $\epsilon_v$ ). As in RE87, we assume on dimensional grounds that  $\epsilon_h = \nu_h^3/l_h^4$  and  $\epsilon_v = \nu_v^3/l_v^4$ , where  $l_h$  and  $l_v$  are length scales of the most energetic turbulent motions (i.e., the energy-containing eddies). From these assumptions, we derive the diagnostic formulas for eddy viscosity:

$$\nu_h = l_h^2 S_h \quad \text{and} \quad \nu_v = l_v^2 (S_v^2 - N_m^2)^{1/2}. \quad (17)$$

We set  $\nu_v = 0$  if  $(S_v^2 - N_m^2) < 0$  (i.e., if the Richardson number is greater than unity).

The formulation of  $N_m^2$  for unsaturated air is given by  $N_m^2 = (g/\theta_v) \partial \theta_v / \partial z$  and for saturated air is given by

$$N_m^2 = \frac{g}{T} \left( \frac{\partial T}{\partial z} + \Gamma_m \right) \left( 1 + \frac{T}{R_d/R_v + q_s} \frac{\partial q_s}{\partial T} \right) - \frac{g}{1 + q_t} \frac{\partial q_t}{\partial z}, \quad (18)$$

where  $q_s$  is the mixing ratio at saturated equilibrium, and  $\Gamma_m$  is the moist-adiabatic lapse rate, which for the conservative equation set is

$$\Gamma_m = g(1 + q_t) \left( \frac{1 + L_v q_s / R_d T}{c_{pm} + L_v \partial q_s / \partial T} \right). \quad (19)$$

To improve energy conservation, dissipative heating can be included in this model. This effect is excluded in most nonhydrostatic numerical models (including the RE87 model), and this option is available herein by setting  $\epsilon = 0$  in (4)–(5). To include this effect with the traditional equation set we use  $\Theta_3 = 1/(c_p \pi)$  and for the conservative equation set we use  $\Theta_3 = c_v/(c_p c_{vm} \pi)$ . For  $\epsilon$ , we use the turbulence kinetic energy balance equation, (15), for the interior of the model domain. At the surface, we utilize the specifications for surface stress and surface fluxes and, using the same assumptions as Bister and Emanuel (1998), we find the dissipation rate at the surface is

$$\epsilon(z=0) = \frac{2C_D}{\Delta z} (u_1^2 + v_1^2)^{3/2} + g \left[ \frac{F_z^\theta}{\theta} + \left( \frac{R_v}{R_d} - 1 \right) F_z^{q_v} \right], \quad (20)$$

where  $C_D$  is the drag coefficient;  $\Delta z$  is the vertical grid spacing;  $u_1$  and  $v_1$  are the radial and azimuthal velocities, respectively, at the lowest model level; and  $F_z^\theta$  and  $F_z^{q_v}$  are the surface fluxes for  $\theta$  and  $q_v$ , respectively. Our formulation for dissipation rate is slightly different from that in previous studies (e.g., Bister and Emanuel 1998; Zhang and Altshuler 1999) because we account for the buoyancy flux [third term on the left side of (15) and the second term of (20)], which typically increases  $\epsilon$  in tropical cyclone eyewalls.

The only significant term associated with energy conservation that has been excluded from this model is one related to sedimentation of liquid water entropy [e.g., last term on the right side of (4.6) in Ooyama (2001)]. This term is excluded herein, which is a traditional assumption in numerical models, because of uncertainties about the best way to formulate the term realistically and yet be computationally efficient [see, e.g., Walko et al. (2000) for a discussion of the difficulty in incorporating this effect realistically]. We are currently investigating this effect further and plan to report our findings in a future study.

### b. Numerical methods

The time integration scheme is third-order Runge–Kutta using split-explicit integration for the acoustic modes, following Wicker and Skamarock (2002). To improve the stability and accuracy of the split-explicit time integration method, we include a weak three-dimensional divergence damper on the acoustic time steps, and we integrate  $\theta$  on the small time steps, following Skamarock and Klemp (1992).

We write the advection terms in flux form for a variable  $\alpha$  as follows:

$$u \frac{\partial \alpha}{\partial r} + w \frac{\partial \alpha}{\partial z} \equiv \frac{1}{r} \frac{\partial (ru\alpha)}{\partial r} + \frac{1}{\bar{\rho}} \frac{\partial (\bar{\rho}w\alpha)}{\partial z} - \alpha \left[ \frac{1}{r} \frac{\partial (ru)}{\partial r} + \frac{1}{\bar{\rho}} \frac{\partial (\bar{\rho}w)}{\partial z} \right]. \quad (21)$$

The first two terms on the right side are discretized using the fifth-order flux-form scheme by Wicker and Skamarock (2002). To conserve total water, we apply a positive-definite scheme [described in Bryan et al. (2006)] to the advection of  $q_v$  and  $q_l$ .

Unlike RE87, we use a closed boundary condition (a rigid wall) at the external lateral boundary, even though an open boundary condition option is available in this code. As compared with an open boundary condition, which is difficult to constrain over long-term integrations, we find a closed boundary produces more stable (i.e., steady) solutions for long-term ( $>10$  day) simulations. To prevent reflection of gravity waves, we apply Newtonian damping to  $u$ ,  $v$ , and  $w$  near this boundary. By comparing it with simulations that use open boundary conditions, we find no significant differences for  $t < 10$  days, but generally more steady conditions in simulations with the closed domain for  $t > 10$  days.

The method to determine  $\dot{q}_{\text{cond}}$  was described by Bryan and Fritsch (2002, p. 2920). As shown in their study, this numerical model does not precisely conserve total mass and energy, partly because of numerical reasons. However, for simulations using the conservative equation set, we find the artificial loss of mass and energy to be several orders of magnitude lower than for simulations using the traditional equation set. At the end of the simulations (typically at  $t = 12$  days), the artificial loss of mass and energy is less than 0.05% of the initial values.

### c. Methodology

The initial conditions are identical to those used by RE87. For the base-state environment, we use their “model neutral” sounding. For our higher-resolution simulations, we interpolate their thermodynamic profile (dots in Fig. 1) to the new grid (lines in Fig. 1), and conditions below their lowest model level are extrapo-

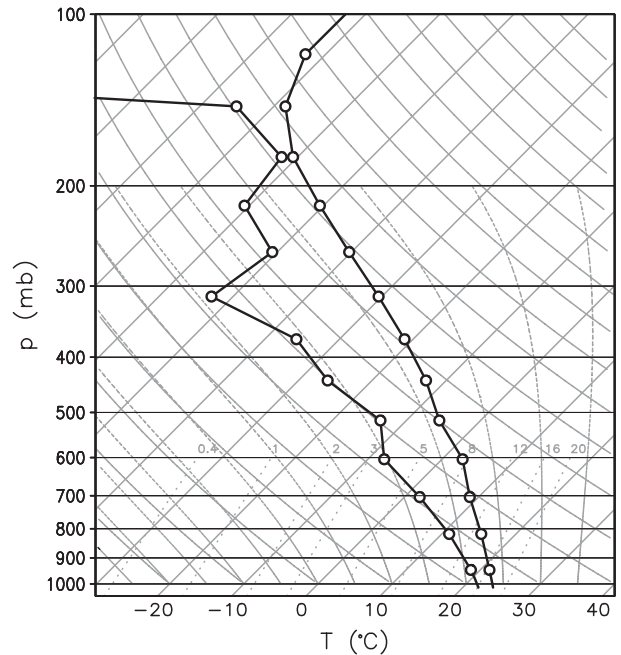


FIG. 1. The thermodynamic sounding used for this study. Dots are the data used in the simulations by RE87, and lines illustrate interpolation (between points) and extrapolation (downward from the lowest model level) to initialize higher-resolution simulations.

lated downward, as shown in this figure. The sea surface temperature ( $T_s$ ) is 26.13°C for all simulations.

The domain is the same size (1500 km  $\times$  25 km) as that used by RE87. Certain settings in the numerical model are varied, depending on the test being conducted, including the grid spacing ( $\Delta r$  for the radial direction,  $\Delta z$  for the vertical direction), the time step ( $\Delta t$ ), and a priori settings for the turbulence parameterization (specifically,  $l_h$  and  $l_v$ ). A summary of model configurations used in this article is presented in Table 1, and further details are provided at appropriate locations later in the text.

Unless stated otherwise, all simulations use the conservative equation set and include dissipative heating, and the surface exchange coefficient for entropy ( $C_E$ ) is equal to that for momentum ( $C_D$ ). (We reiterate that the surface fluxes and stress are formulated the same way as RE87.) The tendency term in the potential temperature equation that mimics radiative cooling ( $R$ ) is capped at 2 K day $^{-1}$  following Experiment J by RE87, which is the same methodology used in all simulations by Persing and Montgomery (2003, hereafter PM03). For all simulations in this article, the parameterization of microphysical processes is identical to that in RE87, and we use  $V_t = 7$  m s $^{-1}$  unless stated otherwise. Ice processes are neglected for the sake of simplicity and because we find they have a small effect on maximum simulated intensity.

TABLE 1. Summary of model parameters for different configurations, where  $\Delta r$  is the radial grid spacing,  $\Delta z$  is the vertical grid spacing,  $\Delta t$  is the time step,  $l_h$  is the horizontal turbulence length scale, and  $l_v$  is the vertical turbulence length scale. Unless specified otherwise, the settings under “default” are used for all results.

Configuration	$\Delta r$ (km)	$\Delta z$ (km)	$\Delta t$ (s)	$l_h$ (m)	$l_v$ (m)
Default	1.0	0.25	7.5	(See text)	(See text)
1x (RE87)	15.0	1.25	20	3000	200
4x (PM03)	3.75	0.3125	5	750	200

In all of our simulations, an approximately steady state is achieved by  $\sim 6$  days into the simulation. We quantify the intensity of the simulated tropical cyclones by  $v_{\max}$ , which is the maximum value of  $v$  (from any grid point in the domain) averaged every time step between  $t = 8$  and 12 days. Typically,  $v_{\max}$  is located at the top of the boundary layer (at  $\sim 1$  km). For other analyses herein, we compute average fields using hourly output from  $t = 8$  to 12 days.

We have compared output from this new model with output from the RE87 model. We find that the RE87 model produces more intense tropical cyclones (by about 10%, as measured by  $v_{\max}$ ). Output from our new model also tends to be steadier over time. Details are provided in the appendix. We attribute these differences primarily to improved governing equations and numerical techniques in the new model.

### 3. Sensitivity tests

We now present the results from several sensitivity tests. The primary focus is the maximum model-produced intensity ( $v_{\max}$ ). We reiterate that initial and boundary conditions are identical for *all* simulations herein, so any differences in  $v_{\max}$  are attributable to numerical model settings. There are a great number of details in the modeling system that we could examine, and it is not our goal to document all possible sensitivities. We focus in this article on model settings that exhibit the most sensitivity from our tests, and also on aspects of the numerical model that have uncertain formulations (including the parameterization of unresolved physical processes such as turbulence, air–sea interaction, and some aspects of microphysics). For the sake of completeness, we list here the model settings we investigated but which had a small effect on  $v_{\max}$ , and thus are not discussed further: ice microphysical processes,<sup>1</sup>

<sup>1</sup> We have conducted simulations using the single-moment scheme of Lin et al. (1983) [as modified for hurricane research by Braun and Tao (2000)] and the double-moment scheme of Morrison et al. (2009).

water conservation (i.e., the use of a positive-definite advection scheme), a larger domain size, the external lateral boundary condition, the size and intensity of the initial vortex, and the “precipitation mass sink” effect (e.g., Qiu et al. 1993; Lackmann and Yablonsky 2004).

As a simple check on the realism of the model output, we compare  $v_{\max}$  to the maximum intensity reported in observational studies. In a study of the Atlantic Ocean, DeMaria and Kaplan (1994) reported a maximum intensity for  $T_s = 26^\circ\text{C}$  of roughly  $50 \text{ m s}^{-1}$ . In a study of the eastern North Pacific, Whitney and Hobgood (1997) reported a maximum intensity of  $61.1 \text{ m s}^{-1}$ . These values are maximum 1-min-sustained wind speeds near the surface, as listed in best-track datasets. For the numerical model,  $v_{\max}$  is a long-term (4 day) averaged value of  $v$  using output from any model grid point, and maximum  $v$  is usually located at the top of the boundary layer (at roughly  $z = 1$  km). Because of the differences, these observed and model-produced measures of intensity are not directly comparable. We note that  $v_{\max}$  tends to be about 20% larger than the wind speed at the top of the surface layer (i.e., at the lowest model level). Kepert (2006a,b) documented a similar profile in  $v$  using observations of two strong hurricanes. So, for the sake of fair comparison, we increase the maximum reported intensity by roughly 20%, and we conclude that  $70 \text{ m s}^{-1}$  is a reasonable estimate for the observation-based analog to  $v_{\max}$  for this sea surface temperature, although we place no significance on small (of order  $5 \text{ m s}^{-1}$ ) differences between this number and  $v_{\max}$ .

We defer a comparison with theoretical estimates of maximum intensity to a later article, because there are so many cases to consider, and because of the difficulty in determining an appropriate theoretical value for each simulation. For now, we note that some of the simulations herein produce  $v_{\max}$  that is significantly greater (by up to 40%) than the theoretical maximum intensity derived by Emanuel (1986), which is consistent with studies using the RE87 model (e.g., PM03; Bryan and Rotunno 2009).

#### a. Grid spacing

Several studies have shown that numerically simulated intensity increases as the horizontal grid spacing decreases (e.g., Braun and Tao 2000; PM03; Yau et al. 2004; Davis et al. 2008; Hill and Lackmann 2009), at least for grid spacing  $\geq 1$  km. Presumably, the ability to better resolve nonhydrostatic processes in the eyewall is the primary reason for this sensitivity.

To determine a nominal grid spacing for this study, we conduct a resolution sensitivity test where we decrease the grid spacing incrementally until a converged value for  $v_{\max}$  is obtained (i.e., until  $v_{\max}$  stops changing). For

these tests, we configure the model to have minimal diffusion by specifying small values for the turbulence length scales: specifically, we use  $l_h = 187.5$  m and  $l_v = 50$  m. From these simulations, we find a converged value for  $v_{\max}$  of  $\sim 100$  m s $^{-1}$  and this magnitude is achieved for approximately  $\Delta r = 1000$  m and  $\Delta z = 250$  m (Table 2); further decreases in either  $\Delta r$  or  $\Delta z$  yield essentially the same intensity. We note that this intensity is significantly larger than the maximum observed value ( $\sim 70$  m s $^{-1}$ ); we analyze and explain this discrepancy later in this article.

Regarding the horizontal grid spacing, we find, similar to previous studies, that the tropical cyclone becomes more intense as the eyewall becomes smaller and better resolved. For  $\Delta r$  of order 1 km or less, the eyewall is represented by at least 8 grid increments; further decreases in  $\Delta r$  do not change the physical width of the eyewall.

Regarding the vertical grid spacing, we find an increase in intensity as  $\Delta z$  increases for this model.<sup>2</sup> In this case, the boundary layer becomes poorly resolved, and becomes artificially deeper, for  $\Delta z \geq 500$  m.

Based on these results, we use  $\Delta r = 1000$  m and  $\Delta z = 250$  m for all results hereafter. Based on further tests (not shown), we find it sufficient to use constant  $\Delta r$  in the inner-core region only, with stretched grid spacing beyond. Specifically, we use  $\Delta r = 1$  km for  $r < 64$  km, and then  $\Delta r$  increases gradually to a maximum value of 16 km at  $r = 1500$  km. Comparison against a simulation with  $\Delta r = 1$  km everywhere yields the same results, so the stretched grid is used hereafter to reduce computational expense.

We remind readers that simulations with an axisymmetric numerical model (and any two-dimensional model) cannot explicitly produce realistic turbulence. Rather, the effects of all turbulence must be included via parameterization. (See the discussion by RE87, p. 544, for more details.) Consequently, the grid spacing used herein cannot be expected to produce a converged solution in a three-dimensional numerical model, where turbulence is parameterized much differently, and can actually be resolved given sufficient resolution [probably with grid spacing of order 100 m, following the theoretical arguments by Bryan et al. (2003)]. Results by Rotunno et al. (2009, manuscript submitted to *Bull. Amer. Meteor. Soc.*) confirm this conclusion.

### b. Turbulence length scales

One of the most uncertain aspects of axisymmetric numerical models is the parameterization of unrepresented motions. In addition to unresolved subgrid-scale

TABLE 2. Maximum azimuthal velocity ( $v_{\max}$ ) from resolution sensitivity tests.

$\Delta r$ (m)	$\Delta z$ (m)	$v_{\max}$ (m s $^{-1}$ )
Sensitivity to $\Delta r$		
16 000	250	70
8000	250	96
4000	250	98
2000	250	100
1000	250	102
500	250	104
Sensitivity to $\Delta z$		
1000	1000	119
1000	500	111
1000	250	102
1000	125	105
1000	63	103

motions, axisymmetric numerical models cannot resolve any three-dimensional motions, such as mesovortices in the eye/eyewall, boundary layer roll vortices, upper-level asymmetric outflow jets, vortex Rossby waves, and so on. Any nonaxisymmetric motions must be viewed as turbulence in an axisymmetric model and must be incorporated through parameterization; see section 2b in RE87 for more details. In this model, turbulence is included via the  $D$  terms in (1)–(7). The turbulence closure (described in section 2) allows for these tendencies to be larger when the local deformation is larger and/or when the local static stability is smaller. Additionally, the closure contains two unknown length scales: one for horizontal turbulence processes ( $l_h$ ) and one for vertical turbulence processes ( $l_v$ ). The  $D$  terms are proportional to  $l_h$  and  $l_v$ , which are specified a priori in this model.

There is no quantitative theoretical guidance for how to set  $l_h$  and  $l_v$  in an axisymmetric model. RE87 used  $l_h = 3000$  m and  $l_v = 200$  m in their simulations, which they determined by trial and error, and by subjective evaluation of model output. PM03 used  $l_h = 750$  m and  $l_v = 200$  m for their standard “4x” setup. A different value for  $l_h$  was used by PM03 because the RE87 model’s code specifies  $l_h$  in terms of a coefficient times the radial grid spacing (specifically, as  $0.2 \times \Delta r$ ), and PM03 used smaller  $\Delta r$  as compared with RE87. Consequently, without any compensating change in the coefficient, RE87’s code has a fundamentally different representation of horizontal turbulence effects as  $\Delta r$  changes, where the turbulent tendencies are *decreased* with higher resolution. However,  $l_h$  should be interpreted as a physical parameter in axisymmetric numerical models, because three-dimensional turbulent motions cannot be resolved at *any* grid spacing; thus, the turbulence length scales should be kept constant for resolution sensitivity tests (as was done in section 3a).

<sup>2</sup> Results could conceivably be different for other numerical models and/or surface layer parameterizations.

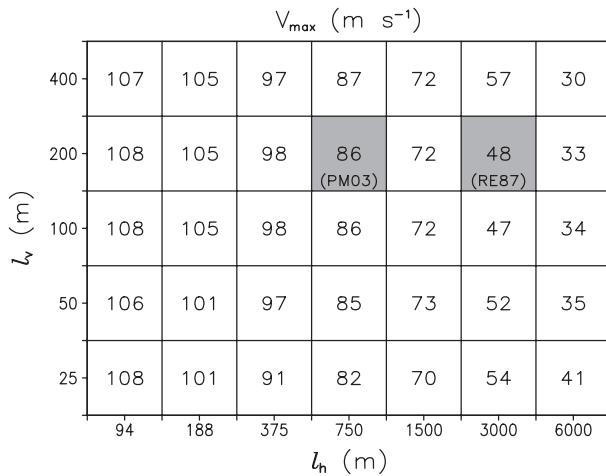


FIG. 2. Maximum azimuthal velocity ( $v_{\max}$ ,  $\text{m s}^{-1}$ ) from simulations that use different values for  $l_h$  and  $l_v$ . Shaded boxes denote settings used by RE87 and PM03.

Here, we evaluate the sensitivity of  $v_{\max}$  to  $l_h$  and  $l_v$  using fixed model parameters (listed as “default” in Table 1). Results, in terms of  $v_{\max}$ , are shown in Fig. 2. There is a strong sensitivity to  $l_h$ , but essentially no sensitivity to  $l_v$ . For  $l_v = 200$  m (the value used by both RE87 and PM03), there is nearly a factor of 2 increase in  $v_{\max}$  when  $l_h$  is decreased from 3000 (the value used by RE87) to 750 m (the value used by PM03). A similar response to changes in  $l_h$  and  $l_v$  (for fixed grid spacing) was reported by PM03 (in their Table 3).

We find from analysis of tendencies in the model’s governing equations (not shown) that with  $l_h$  less than  $\sim 1000$  m the tendency from horizontal turbulence is negligible compared to other terms in the governing equations. So, as  $l_h \rightarrow 0$  the flow becomes essentially inviscid (in the radial direction). To investigate the effects of a truly inviscid model setup, we conduct additional simulations with further decreases in  $l_h$ , including  $l_h = 0$ . Results show that  $v_{\max}$  (solid line in Fig. 3) asymptotically approaches  $113 \text{ m s}^{-1}$  as  $l_h \rightarrow 0$ . For our default model setup, there is additionally a flow-and scale-dependent numerical diffusion that is inherent to the fifth-order advection scheme used herein; this term prevents features from collapsing to a scale smaller than  $\sim 6$  times the grid length. To check the effects of this diffusive term, we also ran a set of simulations (not shown) that uses sixth-order advection, which has no implicit diffusion; these simulations have the same response, although  $v_{\max}$  asymptotically approaches a slightly lower value ( $103 \text{ m s}^{-1}$ ).

These results are somewhat similar to results in Emanuel (1989), who used a balanced axisymmetric model expressed in angular momentum coordinates. Starting with very small diffusion in the lateral direction (his ex-

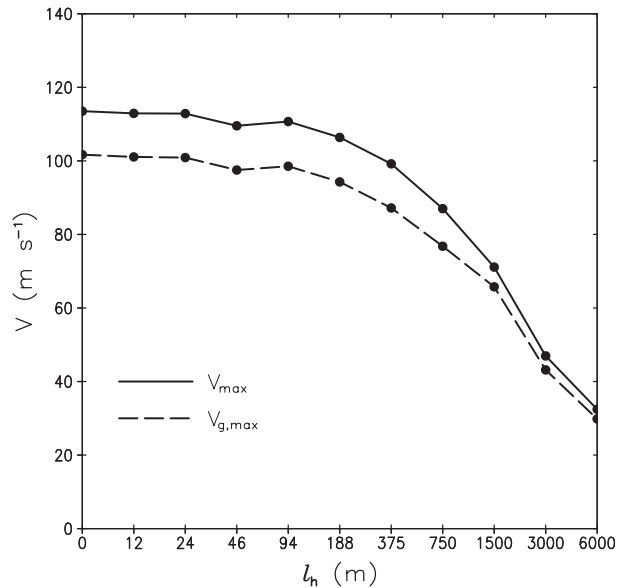


FIG. 3. Maximum azimuthal velocity ( $v_{\max}$ , solid) and maximum gradient wind ( $v_{g,\max}$ , dashed) from simulations that use different values for  $l_h$  (using  $l_v = 200$  m).

periment C1), he found essentially no change in  $v_{\max}$  for a factor-of-3 increase in  $l_h$  (his experiment A), and a slight ( $\sim 10\%$ ) decrease in  $v_{\max}$  for a further factor-of-3 increase in  $l_h$  (his experiment C2, see Fig. 5 in his article). The same behavior is seen in our model for  $l_h \approx 100$  m; K. A. Emanuel (2008, personal communication) has found that further decreases in  $l_h$  (to near zero) in his model result in a slight decrease in  $v_{\max}$ , although this may be attributable to numerical problems with low diffusion or to other differences in these two models.

What is notably different from the results reported by Emanuel (1989) is the maximum intensity, which is near the theoretical PI ( $\sim 60 \text{ m s}^{-1}$ ) in his study. In our case, PI is also roughly  $60 \text{ m s}^{-1}$  (see PM03), but  $v_{\max}$  significantly exceeds this value when  $l_h < 3000$  m. This ability to significantly exceed the theoretical PI for small  $l_h$  appears to be related primarily to the existence of unbalanced flow (which is not possible in Emanuel’s model). In our model, we find that  $v_{\max}$  is close to the maximum gradient wind speed ( $v_{g,\max}$ ) for  $l_h > 1500$  m (Fig. 3), but  $v_{\max}$  notably exceeds  $v_{g,\max}$  as lateral diffusion becomes small. Because of the complexity of this issue, we will address it in a separate article.

Of more interest to this study is that  $v_{\max}$  greatly exceeds the maximum value that has ever been observed for this environment ( $\sim 70 \text{ m s}^{-1}$ , see the beginning of section 3). This only happens in our model when  $l_h$  is small (i.e., when the flow is essentially inviscid in the radial direction). To understand this result further, we note that radial gradients of all model fields are strongly

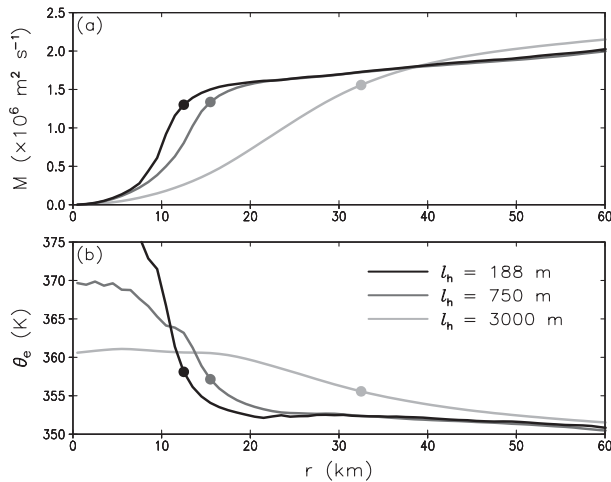


FIG. 4. Properties at the top of the boundary layer ( $z = 1.1 \text{ km}$ ) from simulations that use different values for  $l_h$ , as indicated by the legend (using  $l_v = 200 \text{ m}$ ): (a) angular momentum ( $M$ ), and (b) equivalent potential temperature ( $\theta_e$ ). Dots indicate the location of  $v_{\text{max}}$  in these simulations.

affected by  $l_h$ . Specifically, larger  $l_h$  increases the turbulent diffusion, which yields weaker radial gradients (in both scalar and velocity fields). For example, we show in Fig. 4 the angular momentum ( $M \equiv rv + fr^2/2$ ) and the pseudoadiabatic equivalent potential temperature ( $\theta_e$ ) (Bryan 2008) at the top of the boundary layer. The large differences in  $\theta_e$  in the eye of these simulations (i.e., for  $r < 10 \text{ km}$  in Fig. 4b) are not relevant to the maximum intensity in these simulations, as discussed below. More important are the radial gradients near the location of  $v_{\text{max}}$  (dots in Fig. 4), which are largest for small values of  $l_h$ ; this is because the eyewall of hurricanes is strongly frontogenetic, as discussed by Emanuel (1997). For small  $l_h$ , this frontogenetic zone collapses to a small scale (approximately 8 km wide). But the diffusion terms are frontolytic; thus, as  $l_h$  is increased, and lateral diffusion becomes a significant term in the governing equations, the diffusive terms produce weaker gradients in both scalars and momentum<sup>3</sup> (Fig. 4). Consequently, with large  $l_h$ ,  $M$  from the environment has not been drawn as far into the center of circulation as it can be with smaller  $l_h$ , and thus  $v_{\text{max}}$  is smaller. The weaker radial gradients of scalars are also consistent with weaker intensity because of approximate thermal-wind balance; that is, because  $v \approx 0$  at the top of the troposphere, then weaker shear (consistent with a weaker radial gradient in entropy by thermal wind) must mean weaker intensity.

<sup>3</sup> The same tendency has been found in three-dimensional simulations that explicitly resolve asymmetries (see, e.g., Wang 2002b; Wu and Braun 2004; Yang et al. 2007).

TABLE 3. Properties from simulations with different radial grid spacing ( $\Delta r$ ) using  $l_h = 0$  and  $l_v = 200 \text{ m}$ :  $v_{\text{max}}$  is the maximum azimuthal velocity and  $W$  is the width of the updraft (defined as  $w \geq 0.5 \text{ m s}^{-1}$  at  $z = 1 \text{ km}$ ).

$\Delta r$ (m)	$v_{\text{max}}$ ( $\text{m s}^{-1}$ )	$W$ (km)
16 000	72	32.0
8000	97	16.0
4000	113	8.0
2000	110	8.0
1000	114	9.0
500	114	8.5
250	114	8.5

Based on the preceding arguments, one might wonder whether further increases in resolution would lead to even greater  $v_{\text{max}}$ , because even larger gradients in  $M$  and  $\theta_e$  could be resolved. Our sensitivity studies do not support such a conclusion. Using  $l_h = 0$ ,  $v_{\text{max}}$  is essentially the same for any  $\Delta r < 4 \text{ km}$  (Table 3). In fact, we find that the width of the eyewall, and hence the width of the frontogenetic zone, converges to  $\sim 8 \text{ km}$  for  $\Delta r < 4 \text{ km}$  (Table 3, where the eyewall is defined as  $w \geq 0.5 \text{ m s}^{-1}$ ). The processes that prevent the eyewall from collapsing to an infinitesimal scale (as might be expected for zero turbulent diffusion in a frontogenetic zone) would be an interesting topic for future study, although we surmise that the finite depth of the boundary layer in this model likely plays a role in dictating this finite updraft width.

To help to explain why  $v_{\text{max}}$  is bounded in our simulations, we draw upon the analytic study of tropical cyclone structure and intensity by Emanuel (1986). By assuming gradient-wind balance, hydrostatic balance, and moist slantwise neutrality in the free atmosphere, Emanuel (1986) derived a relationship between the radial gradient of moist entropy ( $s$ ) and the radial gradient of  $M$  in the eyewall [see his Eq. (13)]. If we assume that both  $s$  and  $M$  could collapse to discontinuities in the frontogenetic region of the eyewall, then we can integrate Emanuel's Eq. (13) across the discontinuities, which yields

$$v_{g,\text{max}}^2 = -2(T_B - T_{\text{out}})\Delta s, \quad (22)$$

which is valid only in the eyewall (at the radius of maximum winds), where  $\Delta s$  is the change in  $s$  across the discontinuity,  $T_B$  is temperature at the location of  $v_{g,\text{max}}$ , and  $T_{\text{out}}$  is the “outflow temperature” [which is the temperature, at large radius, along a trajectory that passes through  $v_{g,\text{max}}$  (see Bister and Emanuel 1998, p. 237)]. The important conclusion to be drawn from (22) is that  $v_{g,\text{max}}$  must be finite because  $\Delta s$  must be

finite. Using estimated values of  $T_B$ ,  $T_{\text{out}}$ , and  $\Delta s$  from our weak-diffusion simulations, (22) predicts  $v_{g,\text{max}} \approx 100 \text{ m s}^{-1}$ , which is consistent with  $v_{g,\text{max}}$  from these simulations (Fig. 3). One might wonder what limits the value of  $\Delta s$ , and thus what ultimately limits  $v_{g,\text{max}}$ ; this could be addressed in a future study of theoretical PI.

Returning now to the dependence of model-simulated  $v_{\text{max}}$  on  $l_h$ , our analysis probably explains other simulations of very intense tropical cyclones with axisymmetric numerical models. For example, Hausman et al. (2006) report  $v_{\text{max}}$  exceeding  $130 \text{ m s}^{-1}$  for  $T_s = 28^\circ\text{C}$ . [The maximum observed surface winds for  $T_s = 28^\circ\text{C}$  in the study by DeMaria and Kaplan (1994) was  $\sim 70 \text{ m s}^{-1}$ .] Hausman et al. (2006) had no parameterization for horizontal turbulence in their model (other than the implicit filter in their model's numerics, which is similar to the high-order diffusion used in our model). Their results are consistent with ours, in the sense that essentially inviscid flow leads to very large intensities that are much greater than observed maximum intensities.

Our analysis also explains why PM03 found an increase in intensity with decreasing grid spacing using the RE87 model. As discussed at the beginning of this subsection, their changes in  $\Delta r$  were accompanied by changes in  $l_h$ , the latter of which we find is important for maximum simulated intensity. In contrast, PM03 implicated the existence of high-entropy air in the low-level eye (e.g.,  $r < 10 \text{ km}$  in Fig. 4b); this feature has since been shown to be unimportant for maximum intensity in axisymmetric numerical models [see Bryan and Rotunno (2009) for a detailed analysis], and is thus not discussed further.

One might wonder whether horizontal diffusion of scalars or momentum is more important for changes in  $v_{\text{max}}$ . To investigate, we conduct a series of simulations that calculate different horizontal eddy viscosities for scalars and momentum using a specified horizontal length scale for scalars ( $l_h^s$ ) and one for momentum ( $l_h^m$ ). From a broad set of simulations (not shown here because of space limitations), we find that *both* horizontal diffusion of scalars and momentum is important. If one of these length scales is fixed, and the other is decreased gradually to zero, we again find that  $v_{\text{max}}$  asymptotically approaches a constant, although this constant is different for each experiment. Overall, we find that  $v_{\text{max}}$  is *more sensitive* to changes in  $l_h^m$  than to changes in  $l_h^s$ , although we reiterate that  $v_{\text{max}}$  is sensitive to changes in either length scale.

Before proceeding to other sensitivities in this numerical model, we briefly investigate the hurricane structure as the turbulence coefficients are changed. We show in Fig. 5 the azimuthal and radial flow fields from simulations with three different configurations for tur-

bulence. For relatively large  $l_h$  and  $l_v$  (Fig. 5a), the value of  $v_{\text{max}}$  is  $48 \text{ m s}^{-1}$ , which is less than our estimate for observed maximum intensity ( $70 \text{ m s}^{-1}$ ). The maximum value of radial inflow is  $12 \text{ m s}^{-1}$ , which is comparable to values reported in observed tropical cyclones (e.g., LeeJoice 2000). Overall, for these settings, the model produces features that are reasonably consistent with observational analyses of strong tropical cyclones.

Using smaller  $l_h$ , but the same  $l_v$  (Fig. 5b), the model yields a much smaller radius of maximum winds (as compared to that from the previous model setting). In this case,  $v_{\text{max}}$  is  $86 \text{ m s}^{-1}$ , which is notably larger than our estimate for observed maximum intensity ( $70 \text{ m s}^{-1}$ ); the large discrepancy ( $\sim 15 \text{ m s}^{-1}$ ) raises concerns about the realism of this simulation. Furthermore, consistent with larger values of azimuthal velocities, the maximum value of radial inflow is also larger. In this case, the maximum value of radial inflow is  $\sim 25 \text{ m s}^{-1}$ , which is about twice as large as any value reported by LeeJoice (2000), but is comparable to observations of intense tropical cyclones by Bell and Montgomery (2008) and Kepert (2006a,b). The total depth of radial inflow is  $\sim 2 \text{ km}$  in this simulation, which is slightly higher than, although comparable to, the structure documented in these observational studies. Overall, the structures produced by this model setting can be characterized as extreme, and perhaps unrealistic (at least for  $v_{\text{max}}$ ), compared to available observations.

Using the same (small) value of  $l_h$ , but much smaller  $l_v$ , the maximum azimuthal velocity and the radius of maximum winds remain essentially unchanged (Fig. 5c). However, the depth of the radial inflow is much smaller compared to the previous case. Furthermore, the magnitude of maximum radial inflow is  $40 \text{ m s}^{-1}$ , which is much higher than has been shown in the observational studies cited above. A strong radial *outflow* ( $> 20 \text{ m s}^{-1}$ ) exists at  $z \approx 1.5 \text{ km}$ , which is also much greater than has been previously documented (e.g., Bell and Montgomery 2008). These structures are clearly not representative of natural tropical cyclones. In some simulations with low  $l_h$  and  $l_v$  (although not in this case), inertial instability exists in the eyewall, which is another unnatural feature that can develop in weak-turbulence simulations.

To summarize, the intensity *and* structure of tropical cyclones in axisymmetric numerical models is very sensitive to the specification of turbulence intensity. This means that large uncertainty is an inherent characteristic of axisymmetric numerical model simulations, considering that there is currently no quantitative theoretical guidance with which to specify turbulence effects (particularly in the radial direction). Our analysis further reveals that unnatural features may be produced in an

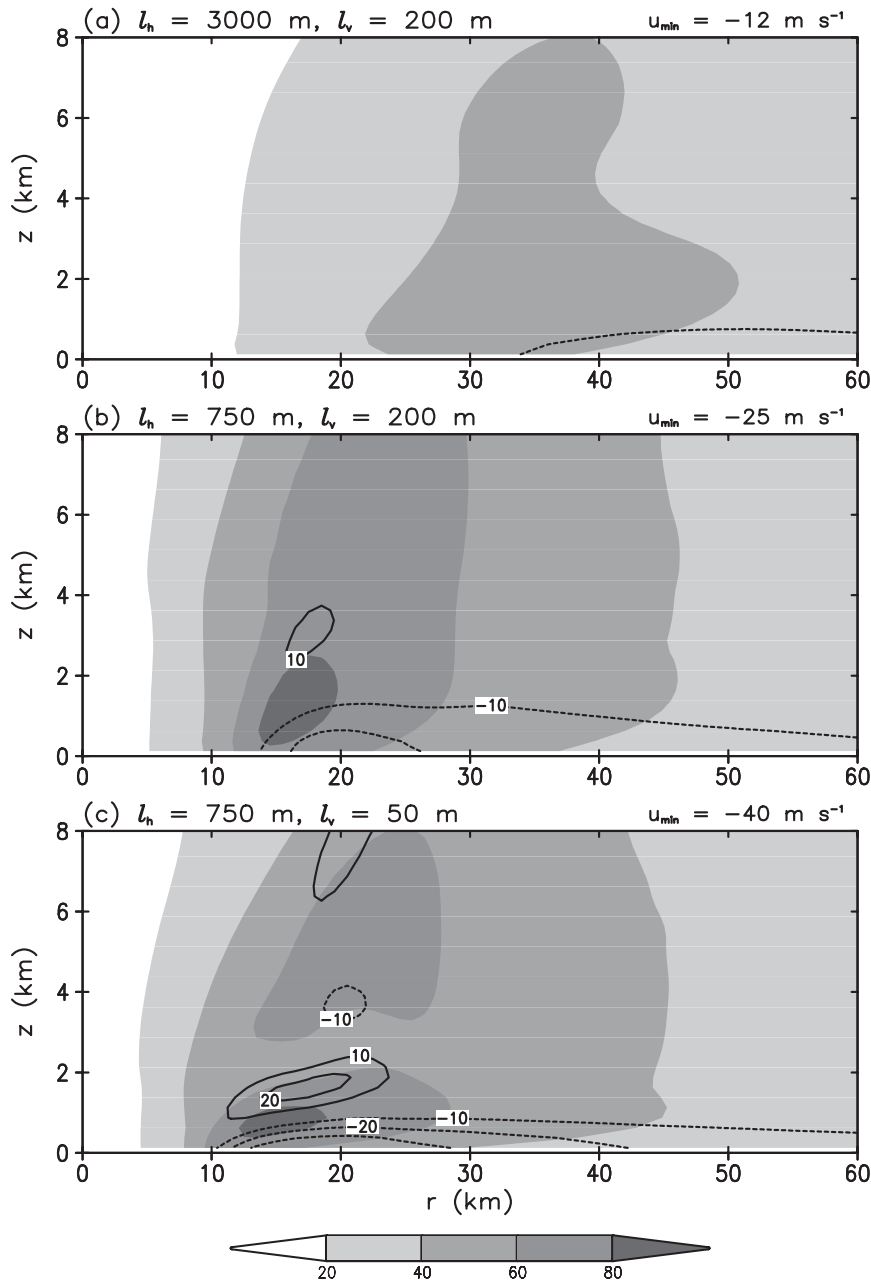


FIG. 5. Output from simulations that use different specification of the turbulence length scales: (a)  $l_h = 3000 \text{ m}$  and  $l_v = 200 \text{ m}$ ; (b)  $l_h = 750 \text{ m}$  and  $l_v = 200 \text{ m}$ ; (c)  $l_h = 750 \text{ m}$  and  $l_v = 50 \text{ m}$ . Azimuthal velocity is shaded and radial velocity is contoured every  $10 \text{ m s}^{-1}$  with negative contours dashed and the zero contour excluded. The minimum value of  $u$  is listed at the top of (a)–(c).

axisymmetric model. As an example,  $v_{\max}$  of  $113 \text{ m s}^{-1}$  (Fig. 3) is clearly unnaturally high as compared to the maximum observed intensity for this sea surface temperature ( $\sim 70 \text{ m s}^{-1}$ ). Consistent with such large azimuthal velocities are unnaturally large values of radial inflow (e.g.,  $|u| > 40 \text{ m s}^{-1}$ ).

Based on these results, we conclude that nearly inviscid axisymmetric model setups (i.e.,  $l_h \rightarrow 0$ ) cannot reproduce realistic tropical cyclones. Furthermore, if  $l_h$  is set to a moderately large value (e.g.,  $3000 \text{ m}$ , which was used by RE87), then no other setup of the numerical model that has been studied herein yields an intensity

larger than the climatologically observed maximum of  $\sim 70 \text{ m s}^{-1}$ .

It follows that turbulence in the radial direction limits axisymmetric tropical cyclone intensity. As discussed earlier, this is because turbulent diffusion weakens the radial gradient of angular momentum in the eyewall (which prevents large values of environmental angular momentum from being drawn to small radius) and also weakens radial gradients of scalars (which consistently means weaker intensity by consideration of thermal-wind balance). Further analysis with three-dimensional models are needed to verify these conclusions, particularly because realistic three-dimensional turbulent flows (e.g., eye/eyewall mesovortices, boundary layer roll vortices, upper-level asymmetric outflow jets, etc.) may act differently than the way they are parameterized in this model.

One might wonder whether we can determine values for  $l_h$  and  $l_v$  that yield reasonably realistic hurricanes as compared to observations. Based on the estimated observed maximum intensity of  $70 \text{ m s}^{-1}$ , as well as comparisons of maximum radial inflow to observations, it seems that  $l_h \approx 1500 \text{ m}$  and  $l_v \approx 100 \text{ m}$  are appropriate. Additionally, observations of azimuthally average properties can be useful in this regards. In an analysis of a category-5 tropical cyclone, Montgomery et al. (2006) found the radial gradient of moist entropy in the eyewall to be  $-1.7 \times 10^{-3} \text{ m s}^{-2} \text{ K}^{-1}$ ; the same value occurs in our simulations if  $l_h = 1500 \text{ m}$ . Despite this encouraging comparison between model output and observations, we cannot say with confidence that these values of  $l_h$  and  $l_v$  will be appropriate for all cases.

As discussed in section 1, a primary goal of this study is to identify the model settings that allow for *maximum possible* intensity in numerical models. Small values of  $l_h$  clearly lead to this goal. Thus, we retain small values of  $l_h$  for the sensitivity tests that follow, although we also present results with  $l_h = 1500 \text{ m}$  as a likely appropriate setting for the comparison against observations.

*c. Ratio of surface exchange coefficients*

Numerical simulations (e.g., Rosenthal 1971; Braun and Tao 2000) and theoretical analysis (e.g., Emanuel 1986, 1995) have demonstrated a large sensitivity of maximum intensity to the ratio of surface exchange coefficients for entropy and momentum ( $C_E/C_D$ ). Observational studies have found that this ratio varies between roughly 0.5 and 1.5, with the lowest values being appropriate for near-surface wind speeds of  $\sim 25 \text{ m s}^{-1}$  (e.g., Black et al. 2007). However, an appropriate value for large wind speeds (of order  $50 \text{ m s}^{-1}$ ) remains uncertain.

To investigate this sensitivity in the numerical model, we set  $C_E = 1.2 \times 10^{-3}$ , based on recent observational

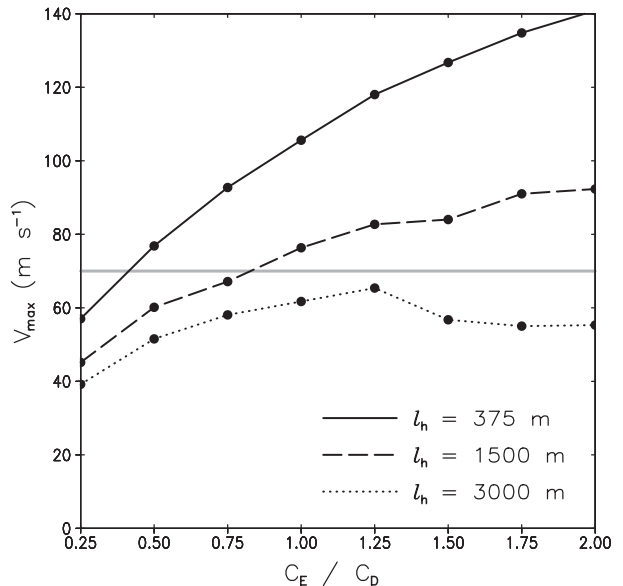


FIG. 6. Maximum azimuthal velocity ( $v_{\max}$ ,  $\text{m s}^{-1}$ ) from simulations that use different ratios of surface exchange coefficients for entropy and momentum,  $C_E/C_D$ , using  $l_h = 375 \text{ m}$  (solid),  $l_h = 1500 \text{ m}$  (dashed), and  $l_h = 3000 \text{ m}$  (dotted). The gray line denotes  $70 \text{ m s}^{-1}$ , which is the approximate maximum intensity observed for this sea surface temperature.

studies (e.g., Drennan et al. 2007). Because  $C_D$  seems to be a more uncertain parameter (e.g., Powell et al. 2003; French et al. 2007), we vary this parameter across a broad range of values. These lower values of both  $C_E$  and  $C_D$  (cf. the default formulations from RE87) result in much slower evolution, and sometimes a steady cyclone does not develop by  $t = 12$  days. Consequently, we double the intensity of the initial vortex (to  $30 \text{ m s}^{-1}$ ) to hasten initial development for this sensitivity test. (These changes to  $C_E$ ,  $C_D$ , and initial vortex intensity were made for this subsection only.) Results for  $C_E/C_D$  between 0.25 and 2 are shown in Fig. 6.

Under the assumption of inviscid flow above the boundary layer, Emanuel (1986, 1995) derived a theoretical relationship,  $v_{\max} \sim (C_E/C_D)^{1/2}$ . For a low value of  $l_h$  in the numerical model (solid line in Fig. 6), we find a similar result:  $v_{\max} \sim (C_E/C_D)^{0.44}$ . For even lower values of  $l_h$  (not shown), we find even closer correspondence to theory; for  $l_h = 94 \text{ m}$ , we find  $v_{\max} \sim (C_E/C_D)^{0.53}$ . Thus, the model results trend toward the theoretical results as turbulence intensity decreases (i.e., as inviscid flow is approached).

In contrast, with higher values of  $l_h$ ,  $v_{\max}$  shows a clearly different dependence. For  $l_h = 1500 \text{ m}$  (dashed line in Fig. 6),  $v_{\max}$  varies as  $(C_E/C_D)^{0.34}$ . For  $l_h = 3000 \text{ m}$  (dotted line in Fig. 6),  $v_{\max}$  varies as  $(C_E/C_D)^{0.31}$  for  $C_E/C_D \leq 1.25$  and  $v_{\max}$  is independent of  $C_E/C_D$  for  $C_E/C_D \geq 1.5$ . Given that nonzero turbulence is needed

in the model to reproduce realistic hurricane structures (see section 3b), these results suggest that viscous terms are needed for an analytical theory of maximum intensity that is appropriate for natural tropical cyclones. Our results might also explain why Braun and Tao (2000) did not find close correspondence between their high-resolution three-dimensional simulations and Emanuel's theoretical model; that is, turbulent diffusion in their model (resolved and/or parameterized) must be relatively important.

As discussed earlier, the approximate maximum intensity of observed tropical cyclones is roughly  $70 \text{ m s}^{-1}$  for this environment. For  $l_h = 375 \text{ m}$ ,  $C_E/C_D$  needs to be less than 0.5 to match this intensity; this seems too low relative to observed values (e.g., Powell et al. 2003; Black et al. 2007), although it could be argued that such low values have never been observed because of difficulties measuring exchange coefficients in high wind speeds. For  $l_h = 1500 \text{ m}$ ,  $v_{\max}$  matches the maximum observed intensity for  $C_E/C_D \approx 0.75$ ; the same conclusion was drawn by Emanuel (1995). For  $l_h = 3000 \text{ m}$ , the model cannot reproduce maximum observed intensity, which suggests that this specification of turbulence intensity is too extreme.

Although the formulation of surface exchange coefficients has been studied often in recent observational campaigns, these results suggest that turbulence in the radial direction is a crucially important parameter that should also be studied further. Indeed, assuming  $l_h = 1500 \text{ m}$  is an appropriate value, then  $v_{\max}$  from this model changes by only  $\sim 25\%$  if the ratio  $C_E/C_D$  is doubled from 0.5 to 1.0 (Fig. 6). In contrast,  $v_{\max}$  can change by 100% for values of  $l_h$  that have been used in published literature (Fig. 2). Further comparison between model results and observations could be undertaken to help to constrain the value of  $l_h$  for axisymmetric models. Additional analyses of the axisymmetric structure of intense tropical cyclones in steady state—such as the analyses presented by Bell and Montgomery (2008)—would be valuable for this purpose. Additionally, a similar study with a three-dimensional numerical model should be conducted to check whether these results are sufficiently general.

#### d. Liquid water fall velocity

We now investigate sensitivity to the specification of terminal fall velocity for liquid water,  $V_t$ . The scheme used herein is the same as that used by RE87, and it is quite simple: if  $q_l$  exceeds  $1 \text{ g kg}^{-1}$ , then this liquid is assumed to fall at  $V_t$ , which by default is  $7 \text{ m s}^{-1}$ . This approach is somewhat unrealistic, but it allows us to document the fundamental response of  $v_{\max}$  to the fall velocity of condensate in an easily understandable manner.

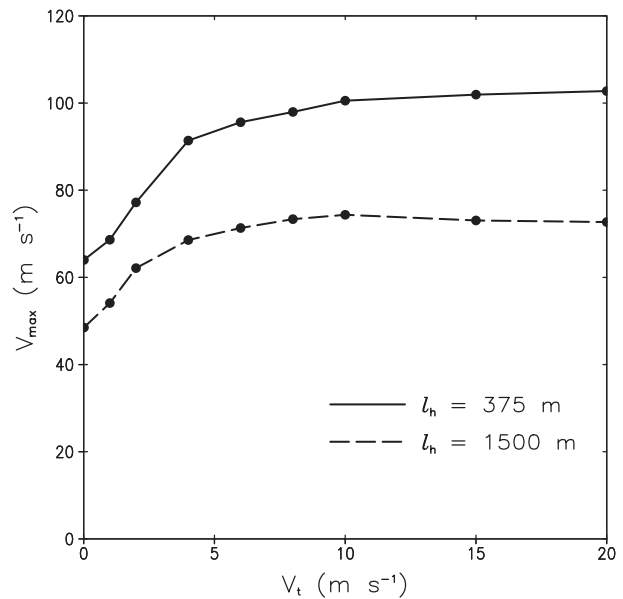


FIG. 7. Maximum azimuthal velocity ( $v_{\max}$ ,  $\text{m s}^{-1}$ ) from simulations that use different values for terminal fall velocity ( $V_t$ ,  $\text{m s}^{-1}$ ) using  $l_h = 375 \text{ m}$  (solid) and  $l_h = 1500 \text{ m}$  (dashed).

Results are shown in Fig. 7 for simulations using  $l_h = 375 \text{ m}$  (solid) and  $l_h = 1500 \text{ m}$  (dashed). We note that this model's governing equations allow for exact reversible thermodynamics when  $V_t = 0$  (in the absence of turbulence effects). This capability is not available in most atmospheric numerical models, which typically neglect terms in the thermodynamical equation (see Bryan and Fritsch 2002).

For reversible thermodynamics ( $V_t = 0$ ), the weakest intensity is produced. As  $V_t$  is increased,  $v_{\max}$  increases, and the intensity for large  $V_t$  is about 60% larger than the reversible case. We also ran simulations (not shown) in which condensate is immediately removed from the atmosphere when  $q_l$  exceeds  $1 \text{ g kg}^{-1}$ ; this is analogous to a pseudoadiabatic process, in which condensate is assumed to immediately fall out from air parcels upon formation. In these latter simulations,  $v_{\max}$  is the same as simulations with large  $V_t$  (Fig. 7).

These results are generally consistent with those from previous studies (e.g., Wang 2002a; Hausman et al. 2006), in the sense that larger fall velocities yield greater intensities. We have also conducted simulations (not shown) with more complex specifications for terminal fall velocity in which  $V_t$  varies proportionally to  $q_l$ , and also simulations that incorporate ice microphysics. From these simulations, we draw the same overall conclusion concerning the correlation between  $v_{\max}$  and  $V_t$  (in which we use a characteristic value of  $V_t$ , such as an average value in the eyewall).

A qualitative consideration of buoyancy helps explain this result. Specifically, larger (positive) buoyancy in a column yields lower perturbation pressure at the bottom of the column;<sup>4</sup> stronger near-surface winds are, of course, consistent with lower pressure. In the simulations with small  $V_t$ , there is a great deal of condensate in the column, which contributes to lower buoyancy, and is thus consistent with weaker intensity. For  $V_t \rightarrow \infty$ , there is no condensate in the column, and thus buoyancy is comparatively higher, which is consistent with stronger intensity. This line of reasoning is supported by the analytic study by Emanuel (1988), who found that an assumption of pseudoadiabatic thermodynamics ( $V_t \rightarrow \infty$ ) yielded much stronger tropical cyclones (by  $\sim 25$  mb, in terms of minimum central pressure) than an assumption of reversible thermodynamics ( $V_t = 0$ ). Emanuel (1988) similarly concluded that water loading plays a key role in reducing the intensity in the reversible case.

To provide further guidance for the development and evaluation of PI theories, we examine the total moist entropy ( $s$ ) from our simulations. In the absence of turbulence effects,  $s$  should be conserved following a parcel. To determine an appropriate mathematical formulation of  $s$ , a further assumption must be made about the liquid water fall velocity. On one extreme, assuming  $V_t = 0$ , an exact expression for  $s$  in reversible conditions—hereafter  $s_r$ —can be derived:

$$s_r = (c_p + c_l r_t) \ln T - R_d \ln p_d + \frac{L_v q_v}{T} - R_v q_v \ln(\mathcal{H}), \quad (23)$$

(e.g., Emanuel 1994), where  $\mathcal{H}$  is relative humidity and  $p_d$  is the partial pressure of dry air. On the other extreme, if liquid water is immediately removed upon formation (i.e., for  $V_t \rightarrow \infty$ ), then a highly accurate expression for  $s$  in pseudoadiabatic conditions—hereafter  $s_p$ —can be derived:

$$s_p = c_p \ln T - R_d \ln p_d + \frac{L_0 q_v}{T} - R_v q_v \ln(\mathcal{H}), \quad (24)$$

(Bryan 2008), where  $L_0 = 2.555 \times 10^6 \text{ J kg}^{-1}$  is a constant.

We show the distribution of  $s$  for three simulations in Fig. 8, where  $s_r$  is shown on the left and  $s_p$  is shown on the right. In all panels, the trajectory for the parcel that passes through  $v_{\text{max}}$  is shown as a thick line. As expected,  $s_r$  is approximately conserved in the free atmosphere (i.e., above the boundary layer) in the simu-

lation with  $V_t = 0$  (Fig. 8a), as revealed by the near equivalence of the trajectory and a contour of  $s_r$ . In contrast,  $s_p$  is clearly not conserved in this case (Fig. 8b), especially when the parcel reaches midlevels and  $q_l$  is relatively large. For  $V_t = 7 \text{ m s}^{-1}$  (which is the value used by RE87 and PM03), neither  $s_r$  nor  $s_p$  are conserved following a parcel (Figs. 8c,d). Consequently, this case would be difficult to analyze analytically, because neither the reversible nor the pseudoadiabatic assumption is truly applicable. For  $V_t = 20 \text{ m s}^{-1}$ ,  $s_r$  is clearly not conserved following a parcel, as expected (Fig. 8e); however,  $s_p$  is conserved well along the trajectory (Fig. 8f), indicating that liquid water is removed sufficiently quickly such that the pseudoadiabatic assumption can be invoked for this case.

These examples reveal that a thermodynamical constraint that is suitable for analytical study can probably only be made for one of the extreme situations (i.e., either reversible or pseudoadiabatic thermodynamics): it seems unlikely that a conserved variable could be formulated for the  $V_t = 7 \text{ m s}^{-1}$  case. If the goal is to study the maximum possible intensity of tropical cyclones, then clearly the pseudoadiabatic assumption should be made. Of course, this state would never be realized in natural tropical cyclones, because the fall velocity of condensate is of order  $5 \text{ m s}^{-1}$  (for liquid condensate, but smaller for snow). Consequently, there is a dilemma that is analogous to the choice for turbulence intensity (section 3b); that is, the pseudoadiabatic assumption may yield the *maximum possible* intensity, but this assumption is clearly not appropriate for natural tropical cyclones.

One might wonder whether the environmental sounding used for these simulations has some affect on these results. The sounding used herein was generated by RE87 to be approximately neutral to convection in their modeling study. With the different governing equations and resolution of this model, it is conceivable that a different result might be obtained for a truly moist-neutral sounding appropriate for our model. Furthermore, by changing the physics of the model from reversible ( $V_t = 0$ ) to pseudoadiabatic ( $V_t \rightarrow \infty$ ), the fixed model atmosphere is clearly no longer neutral to convection across these tests. To investigate, we create two exactly moist-neutral soundings using the model's equations: one for the reversible case (solid line in Fig. 9) and one for the pseudoadiabatic case (dashed line in Fig. 9). Both soundings have exactly zero CAPE under their respective thermodynamical assumption. To be as comparable as possible to the control simulations, we set the surface  $\theta_e$  to be identical to that in the control sounding, and we use a similar tropopause height (15 km). Results using  $l_h = 375 \text{ m}$  are listed in Table 4.

<sup>4</sup> This statement follows from both the hydrostatic equation and from a nonhydrostatic anelastic pressure equation of form  $\nabla^2 \pi' = \partial B / \partial z$ .

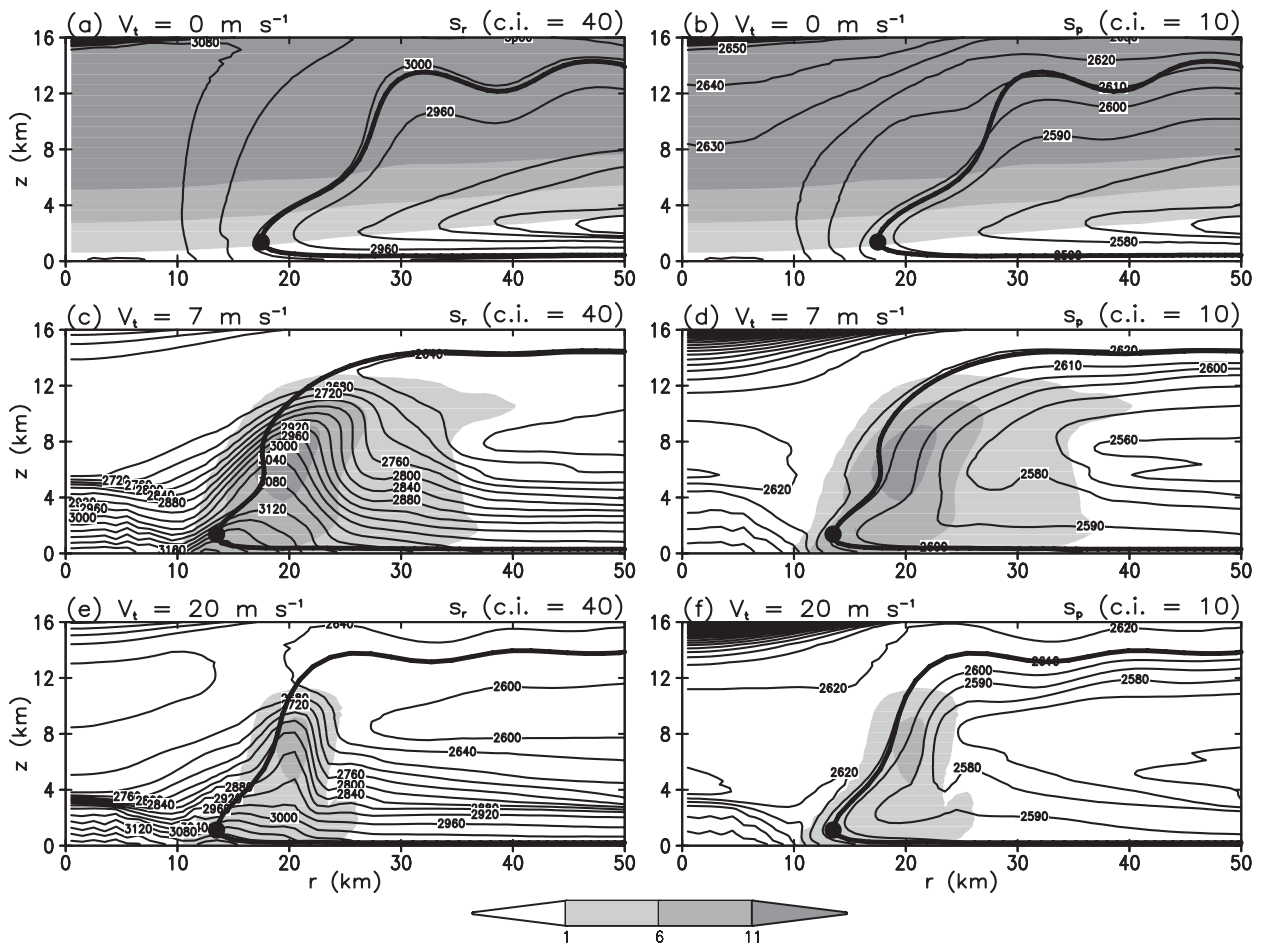


FIG. 8. Analyses of the trajectory that passes through  $v_{\max}$  plotted over  $s$  and  $q_1$  from three simulations that use different fall velocities: (a),(b)  $V_t = 0 \text{ m s}^{-1}$ ; (c),(d)  $V_t = 7 \text{ m s}^{-1}$ ; and (e),(f)  $V_t = 20 \text{ m s}^{-1}$ . The trajectory is illustrated by the thick line, and the dot denotes the location of  $v_{\max}$ . Entropy is contoured:  $s_r$  is on the left (with contour interval of  $40 \text{ J kg}^{-1} \text{ K}^{-1}$ ) and  $s_p$  is on the right (with contour interval of  $10 \text{ J kg}^{-1} \text{ K}^{-1}$ ). Shading denotes  $q_1$  ( $\text{g kg}^{-1}$ ).

Overall, the same conclusion is obtained: reversible thermodynamics yields the weakest intensity and pseudoadiabatic thermodynamics yields the strongest intensity, although for these new soundings the difference is greater. We are unsure, at this time, why the difference in intensity is much larger than that found by theoretical estimates (e.g., Emanuel 1988), which could be a topic for future study.

Finally, we note that these results reveal potential implications for intensity change forecasting, as well as for NWP model development. Specifically, modest changes in  $V_t$  can result in significant changes in tropical cyclone intensity. This is especially the case for  $V_t < 5 \text{ m s}^{-1}$  (Fig. 7) where a change in  $V_t$  of only  $1 \text{ m s}^{-1}$  leads to a change in intensity of  $\sim 10\%$ . Consequently, from a physical perspective, changes in the aerosol content of a tropical cyclone's environment should change  $V_t$ , which might then lead to significant ( $\sim 10\%$ ) changes in

intensity. These microphysical aspects of tropical cyclones might be part of the reason why tropical cyclone intensity has been so difficult to predict operationally.

#### e. Equation set

One unique aspect of this numerical model is the equation set, which mathematically conserves internal energy for reversible moist flows. In contrast, most non-hydrostatic cloud-scale models use an approximate equation set where the heat capacities of water are neglected, which leads to a cold bias when the liquid water content is large (Bryan and Fritsch 2002). For numerical models that do include these effects (e.g., Ooyama 2001; Satoh 2003), it is unclear whether simulations of tropical cyclones are considerably different from simulations that use traditional approximate equation sets. Therefore, in this subsection we investigate the impacts of the different equation sets in our model.

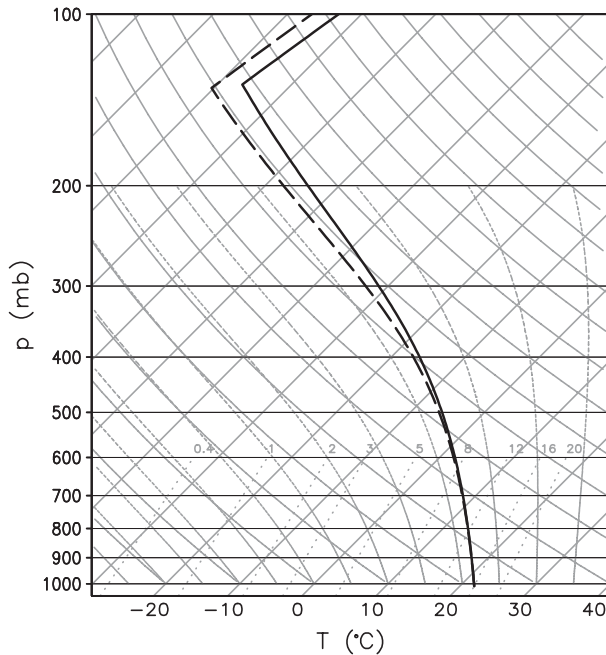


FIG. 9. Thermodynamic soundings used for sensitivity analysis: a reversible sounding (solid) and a pseudoadiabatic sounding (dashed). Both soundings are saturated, and both have the same equivalent potential temperature at the surface as the control sounding.

Figure 10 shows a comparison of  $v_{\max}$  from simulations that use the conservative equation set (solid lines) and simulations that use the traditional equation set (dashed lines). For relatively large fall velocity ( $V_i > 5 \text{ m s}^{-1}$ ), there is essentially no difference in results. This is because the derivation of the traditional equation set is analogous to making the pseudoadiabatic assumption, where liquid water contents are low and thus the heat content of liquid water can be neglected (Bryan 2008). In contrast, for relatively small fall velocity ( $V_i < 5 \text{ m s}^{-1}$ ), the simulations using the traditional equation set are 10%–20% weaker than simulations using the conservative equation set. This result is consistent with the arguments provided in section 3d; that is, lower column-integrated buoyancy yields weaker intensities. In this case, the cool bias incurred by neglecting the specific heats of water leads to the weaker intensities.

#### 4. Summary

In this study, we use an axisymmetric model to investigate the maximum possible intensity of numerically simulated tropical cyclones. The model is designed to conserve total mass and energy in reversible saturated conditions, and uses relatively newly developed nu-

TABLE 4. Maximum azimuthal velocity ( $v_{\max}$ ) from simulations using different environmental soundings and thermodynamics (for  $l_h = 375 \text{ m}$ ).

Setup: Sounding/thermodynamics	$v_{\max}$ ( $\text{m s}^{-1}$ )
Control/reversible	64
Control/pseudoadiabatic	103
Reversible/reversible	40
Pseudoadiabatic/pseudoadiabatic	104

merical techniques. Relative to the axisymmetric model developed by RE87, tropical cyclones in the new model are systematically weaker by  $\sim 10\%$  (see the appendix); this difference is attributed to several approximations made in the Rotunno–Emanuel model.

Sensitivity tests are conducted to determine the model setup that yields maximum sustained azimuthal velocity ( $v_{\max}$ ), and to determine the sensitivity of  $v_{\max}$  to uncertain aspects of the model system. Based on a large set of simulations, we find maximum intensity occurs with the following model setup:

- $\Delta r \approx 1 \text{ km}$  or less and  $\Delta z \approx 250 \text{ m}$  or less,
- inviscid flow in the radial direction,
- pseudoadiabatic thermodynamics (i.e., hydrometeor fall velocities greater than  $\sim 10 \text{ m s}^{-1}$ ), and
- an equation set that conserves internal energy (if hydrometeor fall velocities are of order  $1 \text{ m s}^{-1}$ ).

These findings should be useful for the development of analytical models of maximum intensity. However, we note that some of these model settings yield unnatural structures, as compared to available observations of axisymmetric tropical cyclone structure. For example, the simulations with essentially inviscid flow produce inflow velocities and azimuthal velocities that have never been documented with observations; the maximum azimuthal velocity exceeds  $119 \text{ m s}^{-1}$ , which is much greater than the maximum observed value ( $\sim 70 \text{ m s}^{-1}$ ) for this environment. Thus, some of these settings are clearly unnatural. Indeed, it is quite obvious that natural tropical cyclones are not inviscid, and that pseudoadiabatic thermodynamics are not applicable. This poses a problem for development of analytic models of maximum intensity, because the governing equations for such extreme assumptions are the most simple, and thus most tractable, for analytic development.

The intensity and structure of the simulated tropical cyclones is *most* sensitive to the specification of turbulence intensity. In particular, turbulence in the radial direction limits maximum intensity because it reduces the radial gradient of angular momentum in the eyewall (which prevents large values of environmental angular momentum from being drawn to small radius) and

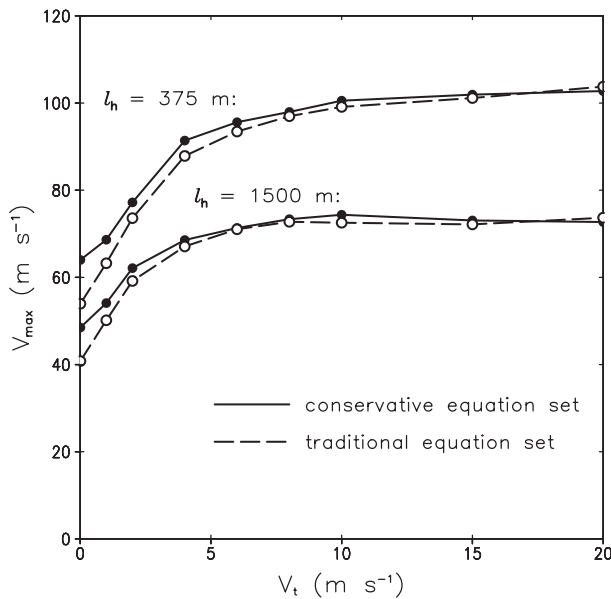


FIG. 10. As in Fig. 7, except that the solid line shows results using the conservative equation set and the dashed line shows results using the traditional equation set. The upper set of curves use  $l_h = 375$  m and the lower set of curves use  $l_h = 1500$  m.

turbulence also reduces radial gradients of scalars (which is consistent with weaker intensity, owing to approximate thermal wind balance). Unfortunately, the parameterization of turbulence is the most uncertain aspect of axisymmetric models; there is no theory for how to formulate the intensity of turbulence in this framework, and few observations are available to constrain the adjustable settings (e.g.,  $l_h$  and  $l_v$ ) in the model of turbulence used herein. Based on a cursory comparison with observations, we find that  $l_h \approx 1500$  m and  $l_v \approx 100$  m are reasonable settings. Additional high-resolution observations within the eyewall of steady tropical cyclones, such as those presented by Bell and Montgomery (2008), would be needed to gain more confidence in these turbulence settings.

An analytic model that assumes inviscid flow above the boundary layer (Emanuel 1986, 1995) found that maximum intensity is proportional to the ratio of surface exchange coefficients for entropy and momentum:  $v_{max} \sim (C_E/C_D)^{1/2}$ . This result is approximately reproduced for the essentially inviscid model setup. However, for greater intensity of turbulence, the model-produced  $v_{max}$  shows less sensitivity to  $C_E/C_D$ . These results suggest that the ratio  $C_E/C_D$  might be less important to tropical cyclone intensity than previous studies have suggested.

Finally, it seems possible that the difficulty in real-time forecasts of intensity may be partly related to the specification of turbulence in NWP models and/or the

general lack of understanding of turbulence effects in hurricanes. We recommend an examination of turbulence parameterizations in NWP models as a possible fruitful avenue of research. However, three-dimensional large eddy simulation (LES), such as that conducted by Rotunno et al. (2009, manuscript submitted to *Bull. Amer. Meteor. Soc.*) might be needed to fully understand the effects of turbulence on hurricane intensity, because high-resolution LES is insensitive (in principle) to modest changes in the subgrid turbulence parameterization.

*Acknowledgments.* The authors thank Chris Davis, Greg Holland, and Morris Weisman for providing reviews of an earlier version of this manuscript, and Kerry Emanuel, Yuqing Wang, and an anonymous reviewer for their formal reviews of this manuscript. All figures were created using the Grid Analysis and Display System (GrADS).

## APPENDIX

### Comparison with the RE87 Model

Here we compare results from the new model (hereafter the BR model) with results from the RE87 model. This comparison helps put the new model's results into context with previously published results (e.g., RE87; Bister and Emanuel 1998; PM03), and it also serves as a cursory check of the model's accuracy. For these tests, we use two settings: 1) the settings used by RE87, hereafter referred to as the 1x configuration; and 2) the settings used in the 4x simulations by PM03, where grid spacing (in both directions) is reduced by a factor of 4, the time step is reduced by a factor of 4, and  $l_h$  is reduced by a factor of 4, relative to the 1x configuration (see Table 1). We use  $V_i = 7$  m s<sup>-1</sup> for all simulations (as in RE87). For simulations with the BR model, we use the conservative equation set, although for this value of  $V_i$  the impact of this different equation set is minimal (Fig. 10). We neglect dissipative heating for these tests because it is not included in the RE87 model. Consequently, these tests primarily evaluate the differences that are attributable to numerical techniques and other seemingly minor differences, as explained below.

Time series of  $v_{max}$  (Fig. A1) reveal two primary differences in model output. First, the BR model generally produces solutions that are steadier for a longer period of time, whereas the RE87 model output drifts more noticeably after roughly 10 days. In this case, the RE87 model output drifts upward with the 1x configuration, but drifts downward with the 4x configuration; the same general result was documented by Persing and

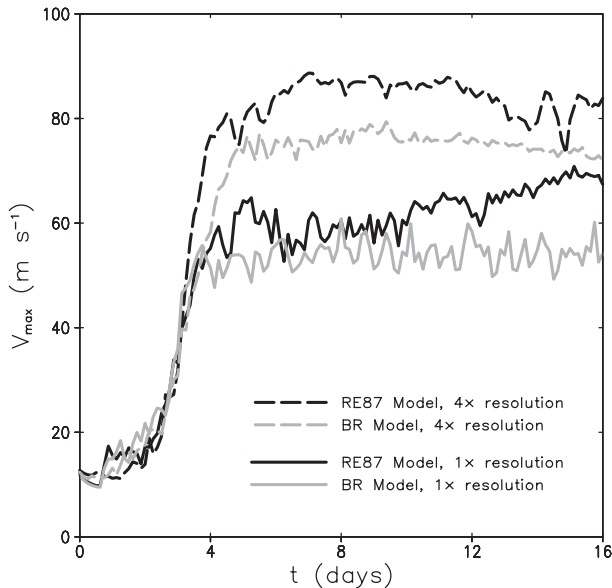


FIG. A1. Time series of maximum azimuthal velocity ( $v_{\max}$ ,  $\text{m s}^{-1}$ ) from two models at two different resolutions, as indicated by the legend. To provide a smoother analysis, data are averaged over 3 h.

Montgomery (2005). A slight weakening trend occurs with the BR model, especially for the 4x setup; however, with the 4x configuration, the downward trend between days 8–16 is a factor of 2 smaller than with the RE87 model. We attribute the steadier solutions to improvements in the BR model, particularly with regards to mass conservation and the more accurate numerical techniques, but also to the different lateral boundary condition (discussed in section 2b).

The second primary difference is weaker intensities with the BR model (Fig. A1). Overall,  $v_{\max}$  from the BR model is about 10% smaller than  $v_{\max}$  from the RE87 model. This result is difficult to explain. To gain insight, we ran a multitude of test simulations with the BR model using the 4x configuration in which we modified the governing equations, numerical techniques, and physical constants to be like those in the RE87 model in an attempt to reproduce the greater intensity. We made too many changes to document in detail herein. Overall, we find that *some* changes to the BR model caused slightly weaker intensities, but that *most* changes we investigated caused slightly stronger intensities when implemented into the BR model. Thus, several approximations in the RE87 model have small positive contributions to intensity, and that the overall effect is a notable ( $\sim 10\%$ ) positive contribution. To demonstrate, we list three modifications in Table A1 that we made to the BR model for which we find a notable positive impact on intensity; also listed in this table is  $v_{\max}$  when

TABLE A1. Maximum azimuthal velocity ( $v_{\max}$ ) from different model configurations. The 4x setup (see Table 1) is used for all simulations.

Model configuration	Description	$v_{\max}$ ( $\text{m s}^{-1}$ )
RE87	Unmodified	86.5
BR	Unmodified	77.8
BR-A	Uses constants from the RE87 model	80.0
BR-B	Uses linearized pressure gradient	79.1
BR-C	Uses second-order advection	79.4
BR-ABC	A + B + C	83.1

using the unmodified versions of the BR and RE87 models. For these tests, we use the 4x configuration (Table 1). The changes are explained in the next several paragraphs.

First, we only modified the values of physical constants in the model. The default values for both models are listed in Table A2. We also modified the formulation of the saturation vapor pressure; the RE87 model uses the formulation from Klemp and Wilhelmson (1978), whereas the BR model uses the formulation from Bolton (1980). The values/formulations that are default in the BR model come from more recent references, and thus are believed to be more accurate. In this test, hereafter BR-A, we find a small ( $+2.2 \text{ m s}^{-1}$ ) increase in intensity (Table A1).

Second, we only modified the pressure gradient term. (We did not retain the changes from the previous paragraph for this test.) The BR model uses the unapproximated form,  $-c_p \theta_v \nabla \pi'$ . The RE87 model uses a linearization whereby  $\theta_v$  is replaced by the base-state value,  $\bar{\theta}_v$ . In this test, hereafter BR-B, we find a small ( $+1.3 \text{ m s}^{-1}$ ) but positive increase in intensity (Table A1).

Third, we only modified the formulation of the advection terms to be second order, instead of fifth order, although the BR model uses a flux form for the advection terms whereas the RE87 model uses an advective form. (Again, we did not retain changes from the previous paragraphs.) In this test, hereafter BR-C, we find a small ( $+1.6 \text{ m s}^{-1}$ ) but positive increase in intensity (Table A1).

When we incorporate all three of these changes in a single test, hereafter BR-ABC, we find an intensity increase of  $+5.3 \text{ m s}^{-1}$  (Table A1), or roughly a 7% increase in intensity. These changes seem to explain most of the discrepancy between the BR model and the RE87 model. More generally, we conclude that a series of reasonable approximations, that by themselves may be small and insignificant, can together act to create a more substantial difference in simulated tropical cyclone

TABLE A2. Default values for constants in the two numerical models.

Symbol	Description (units)	BR value	RE87 value
$c_l$	Specific heat of liquid water ( $\text{J kg}^{-1} \text{K}^{-1}$ )	4190.0	0
$c_p$	Specific heat of dry air at constant pressure ( $\text{J kg}^{-1} \text{K}^{-1}$ )	1005.7	1005.0
$c_{pv}$	Specific heat of water vapor at constant pressure ( $\text{J kg}^{-1} \text{K}^{-1}$ )	1870.0	0
$c_v$	Specific heat of dry air at constant volume ( $\text{J kg}^{-1} \text{K}^{-1}$ )	718.66	718.0
$c_{vv}$	Specific heat of water vapor at constant volume ( $\text{J kg}^{-1} \text{K}^{-1}$ )	1408.5	0
$dL_v/dT$	Temperature dependence of $L_v$ ( $\text{J kg}^{-1} \text{K}^{-1}$ )	$c_{pv} - c_l$	0
$L_v(T_0)$	Latent heat of vaporization at $T = T_0$ ( $\text{J kg}^{-1}$ )	$2.501 \times 10^6$	$2.513 \times 10^6$
$R$	Dry air gas constant ( $\text{J kg}^{-1} \text{K}^{-1}$ )	287.04	287.0
$R_v$	Water vapor gas constant ( $\text{J kg}^{-1} \text{K}^{-1}$ )	461.5	461.4
$T_0$	Reference temperature (K)	273.15	273.0

intensity. We further conclude that several such approximations bias the RE87 model toward comparatively stronger intensities.

#### REFERENCES

- Bell, M. M., and M. T. Montgomery, 2008: Observed structure, evolution, and potential intensity of category 5 Hurricane Isabel (2003) from 12 to 14 September. *Mon. Wea. Rev.*, **136**, 2023–2046.
- Bister, M., and K. A. Emanuel, 1998: Dissipative heating and hurricane intensity. *Meteor. Atmos. Phys.*, **65**, 233–240.
- Black, P. G., and Coauthors, 2007: Air–sea exchange in hurricanes: Synthesis of observations from the Coupled Boundary Layer Air–Sea Transfer Experiment. *Bull. Amer. Meteor. Soc.*, **88**, 357–374.
- Bolton, D., 1980: The computation of equivalent potential temperature. *Mon. Wea. Rev.*, **108**, 1046–1053.
- Braun, S. A., and W.-K. Tao, 2000: Sensitivity of high-resolution simulations of Hurricane Bob (1991) to planetary boundary layer parameterizations. *Mon. Wea. Rev.*, **128**, 3941–3961.
- Bryan, G. H., 2008: On the computation of pseudoadiabatic entropy and equivalent potential temperature. *Mon. Wea. Rev.*, **136**, 5239–5245.
- , and J. M. Fritsch, 2002: A benchmark simulation for moist nonhydrostatic numerical models. *Mon. Wea. Rev.*, **130**, 2917–2928.
- , and R. Rotunno, 2009: The influence of near-surface, high-entropy air in hurricane eyes on maximum hurricane intensity. *J. Atmos. Sci.*, **66**, 148–158.
- , J. C. Wyngaard, and J. M. Fritsch, 2003: Resolution requirements for the simulation of deep moist convection. *Mon. Wea. Rev.*, **131**, 2394–2416.
- , J. C. Knievel, and M. D. Parker, 2006: A multimodel assessment of RKW theory’s relevance to squall-line characteristics. *Mon. Wea. Rev.*, **134**, 2772–2792.
- Davis, C., and Coauthors, 2008: Prediction of landfalling hurricanes with the advanced hurricane WRF model. *Mon. Wea. Rev.*, **136**, 1990–2005.
- DeMaria, M., and J. Kaplan, 1994: Sea surface temperature and the maximum intensity of Atlantic tropical cyclones. *J. Climate*, **7**, 1324–1334.
- Drennan, W. M., J. A. Zhang, J. R. French, C. McCormick, and P. G. Black, 2007: Turbulent fluxes in the hurricane boundary layer. Part I: Latent heat flux. *J. Atmos. Sci.*, **64**, 1103–1115.
- Emanuel, K. A., 1986: An air–sea interaction theory for tropical cyclones. Part II: Steady-state maintenance. *J. Atmos. Sci.*, **43**, 585–604.
- , 1988: The maximum intensity of hurricanes. *J. Atmos. Sci.*, **45**, 1143–1155.
- , 1989: The finite-amplitude nature of tropical cyclogenesis. *J. Atmos. Sci.*, **46**, 3431–3456.
- , 1994: *Atmospheric Convection*. Oxford, 580 pp.
- , 1995: Sensitivity of tropical cyclones to surface exchange coefficients and a revised steady-state model incorporating eye dynamics. *J. Atmos. Sci.*, **52**, 3969–3976.
- , 1997: Some aspects of hurricane inner-core dynamics and energetics. *J. Atmos. Sci.*, **54**, 1014–1026.
- French, J. R., W. M. Drennan, J. A. Zhang, and P. G. Black, 2007: Turbulent fluxes in the hurricane boundary layer. Part I: Momentum flux. *J. Atmos. Sci.*, **64**, 1089–1102.
- Hausman, S. A., K. V. Ooyama, and W. H. Schubert, 2006: Potential vorticity structure of simulated hurricanes. *J. Atmos. Sci.*, **63**, 87–108.
- Hill, K. A., and G. M. Lackmann, 2009: Analysis of idealized tropical cyclone simulations using the Weather Research and Forecasting Model: Sensitivity to turbulence parameterization and grid spacing. *Mon. Wea. Rev.*, **137**, 745–765.
- Holland, G. J., 1997: The maximum potential intensity of tropical cyclones. *J. Atmos. Sci.*, **54**, 2519–2541.
- Kepert, J. D., 2006a: Observed boundary layer wind structure and balance in the hurricane core. Part I: Hurricane Georges. *J. Atmos. Sci.*, **63**, 2169–2193.
- , 2006b: Observed boundary layer wind structure and balance in the hurricane core. Part II: Hurricane Mitch. *J. Atmos. Sci.*, **63**, 2194–2211.
- Klemp, J. B., and R. B. Wilhelmson, 1978: The simulation of three-dimensional convective storm dynamics. *J. Atmos. Sci.*, **35**, 1070–1096.
- Lackmann, G. M., and R. M. Yablonsky, 2004: The importance of the precipitation mass sink in tropical cyclones and other heavily precipitating systems. *J. Atmos. Sci.*, **61**, 1674–1692.
- LeeJoice, R. N., 2000: Hurricane inner-core structure as revealed by GPS dropwindsondes. M.S. thesis, Department of Atmospheric Science, Colorado State University, 56 pp.
- Lin, Y.-L., R. D. Farley, and H. D. Orville, 1983: Bulk parameterization of the snow field in a cloud model. *J. Climate Appl. Meteor.*, **22**, 1065–1092.
- Montgomery, M. T., M. M. Bell, S. D. Aberson, and M. L. Black, 2006: Hurricane Isabel (2003): New insights into the physics of intense storms. Part I: Mean vortex structure and maximum intensity estimates. *Bull. Amer. Meteor. Soc.*, **87**, 1335–1347.
- Morrison, H., G. Thompson, and V. Tatarskii, 2009: Impact of cloud microphysics on the development of trailing stratiform precipitation in a simulated squall line: Comparison of one- and two-moment schemes. *Mon. Wea. Rev.*, **137**, 991–1007.

- Ooyama, K. V., 2001: A dynamic and thermodynamic foundation for modeling the moist atmosphere with parameterized microphysics. *J. Atmos. Sci.*, **58**, 2073–2102.
- Persing, J., and M. T. Montgomery, 2003: Hurricane superintensity. *J. Atmos. Sci.*, **60**, 2349–2371.
- , and —, 2005: Is environmental CAPE important in the determination of maximum possible hurricane intensity? *J. Atmos. Sci.*, **62**, 542–550.
- Powell, M. D., P. J. Vickery, and T. A. Reinhold, 2003: Reduced drag coefficient for high wind speeds in tropical cyclones. *Nature*, **422**, 279–283.
- Qiu, C.-J., J.-W. Bao, and Q. Xu, 1993: Is the mass sink due to precipitation negligible? *Mon. Wea. Rev.*, **121**, 853–857.
- Rosenthal, S. L., 1971: The response of a tropical cyclone model to variations in boundary layer parameters, initial conditions, lateral boundary conditions, and domain size. *Mon. Wea. Rev.*, **99**, 767–777.
- Rotunno, R., and K. A. Emanuel, 1987: An air-sea interaction theory for tropical cyclones. Part II: Evolutionary study using a nonhydrostatic axisymmetric numerical model. *J. Atmos. Sci.*, **44**, 542–561.
- Satoh, M., 2003: Conservative scheme for a compressible nonhydrostatic model with moist processes. *Mon. Wea. Rev.*, **131**, 1033–1050.
- Skamarock, W. C., and J. B. Klemp, 1992: The stability of time-split numerical methods for the hydrostatic and the nonhydrostatic elastic equations. *Mon. Wea. Rev.*, **120**, 2109–2127.
- Walko, R. L., W. R. Cotton, G. Feingold, and B. Stevens, 2000: Efficient computation of vapor and heat diffusion between hydrometeors in a numerical model. *Atmos. Res.*, **53**, 171–183.
- Wang, Y., 2002a: An explicit simulation of tropical cyclones with a triply nested movable mesh primitive equation model: TCM3. Part II: Model refinements and sensitivity to cloud microphysics parameterization. *Mon. Wea. Rev.*, **130**, 3022–3036.
- , 2002b: Vortex Rossby waves in a numerically simulated tropical cyclone. Part II: The role in tropical cyclone structure and intensity changes. *J. Atmos. Sci.*, **59**, 1239–1262.
- Whitney, L. D., and J. S. Hobgood, 1997: The relationship between sea surface temperatures and maximum intensities of tropical cyclones in the Eastern North Pacific. *J. Climate*, **10**, 2921–2930.
- Wicker, L. J., and W. C. Skamarock, 2002: Time splitting methods for elastic models using forward time schemes. *Mon. Wea. Rev.*, **130**, 2088–2097.
- Wu, L., and S. A. Braun, 2004: Effects of environmentally induced asymmetries on hurricane intensity: A numerical study. *J. Atmos. Sci.*, **61**, 3065–3081.
- Yang, B., Y. Wang, and B. Wang, 2007: The effect of internally generated inner-core asymmetries on tropical cyclone potential intensity. *J. Atmos. Sci.*, **64**, 1165–1188.
- Yau, M. K., Y. Liu, D.-L. Zhang, and Y. Chen, 2004: A multiscale numerical study of Hurricane Andrew (1992). Part VI: Small-scale inner-core structures and wind streaks. *Mon. Wea. Rev.*, **132**, 1410–1433.
- Zeng, Z., Y. Wang, and C.-C. Wu, 2007: Environmental dynamical control of tropical cyclone intensity—An observational study. *Mon. Wea. Rev.*, **135**, 38–59.
- Zhang, D.-L., and E. Altshuler, 1999: The effects of dissipative heating on hurricane intensity. *Mon. Wea. Rev.*, **127**, 3032–3038.